# 11 VISCOPLASTICITY

THE elastoplastic constitutive theories presented so far in Part Two of this book are classed as *rate independent* or *time independent*; that is, the material response is regarded as independent of the rate of application of loads and/or the timescale of the problems considered. Time (or, more precisely, *pseudo-time*) is used merely to describe the sequence of events that defines the history of the loading process. For such theories, identical solutions are produced when a given load (or sequence of loads) is applied at different rates.

However, the observed behaviour of real materials is generally time dependent; that is, the stress response always depends on the rate of loading and/or the timescale considered. The extent of such dependence may or may not be significant according to the physical conditions of the problem. In situations where the rates of loading and/or the timescale of the analysis remain within a range where the time-dependent phenomena can be neglected, rate-independent elastoplasticity models can provide good descriptions of the material behaviour (Lemaitre and Chaboche, 1990; Lubliner, 1990; Skrzypek, 1993). If such conditions are not met, then accurate predictions can only be obtained if rate dependence is adequately accounted for by the constitutive model. Rate-dependence effects are described by means of so-called *viscoplasticity* (or *rate-dependent plasticity*) models, to which the present chapter is devoted.

This chapter is organised as follows. Section 11.1 presents a brief introduction to phenomenological aspects of viscoplasticity. It motivates the establishment of a one-dimensional mathematical model of viscoplasticity in Section 11.2. Here, some simple analytical solutions are presented to demonstrate the ability of the one-dimensional model in capturing the fundamental phenomenological features of viscoplastic behaviour. In Section 11.3 the one-dimensional viscoplastic theory is generalised to the multidimensional case within the context of von Mises plasticity. A more general multidimensional model is presented in Section 11.4. The general model can be rigorously described within the constitutive framework of internal variable theories initially referred to in Chapter 3 (Section 3.5.2, from page 71). Rate-independent plasticity is shown to be, under some circumstances, a limit case of the general viscoplasticity model. This establishes a formal link between rate-independent plasticity and the general constitutive framework of Chapter 3. Section 11.5 proceeds to introduce a numerical framework to treat the general viscoplasticity model within the finite element environment of Chapter 4. This includes the numerical integration algorithm for the general viscoplastic constitutive equations as well as a symbolic form of the associated consistent tangent modulus. Then, in Section 11.6, the general numerical framework is specialised to a von Mises-based model presented in Section 11.3. The integration algorithm and the associated consistent tangent operator are derived step by step. In addition, an error assessment of the numerical integration procedure is presented by means of iso-error maps.

*Computational Methods for Plasticity: Theory and Applications* EA de Souza Neto, D Perić and DRJ Owen

We remark that Section 11.6 is essential for the reader interested in the computational implementation of viscoplasticity. The chapter ends with finite element examples being shown in Section 11.7. In the reported examples, the procedures of Section 11.6 are used.

## 11.1. Viscoplasticity: phenomenological aspects

Many of the microscopic phenomena underlying the inelastic deformation of solids depend on time. Materials such as metals, rubbers, geomaterials in general, concrete and composites may all present substantially time-dependent mechanical behaviour under many practical circumstances. In metals, for instance, the phenomenological effects of time-dependent mechanisms become apparent typically at absolute temperatures higher than around one third of the melting point and can be clearly identified by a number of experimental procedures. To illustrate this fact, typical results of simple uniaxial tension tests with metallic bars at higher temperatures are schematically represented in Figure 11.1. Figure 11.1(a) shows stress–strain curves obtained in uniaxial tensile tests carried out under different prescribed strain rates. In general, the elasticity modulus is largely independent of the rate of loading but, clearly, the initial yield limit as well as the hardening curve depend strongly on the rate of straining. This rate-dependence is also observed at low temperatures, but usually becomes significant only at higher temperatures. Strain-rate dependence may be of crucial importance, for instance, in metal-forming operations such as hot forging and may have to be taken into consideration in the design of the process. It is also important to emphasise that, although not shown in Figure 11.1(a), the rupture limit, that is, the strain at which the specimen breaks, can also be strongly dependent on the rate of straining.

Another aspect of time dependence is the phenomenon of *creep*. This is illustrated in Figure 11.1(b). The curves of Figure 11.1(b) show the evolution of plastic strains over time in experiments where tensile specimens have been loaded to different stress levels and left at constant stress during long periods of time. The material experiences a continuous plastic flow that is accelerated for higher stress levels. The high strain rates shown towards the end of the schematic curves for high and moderate stresses is the phenomenon known as *tertiary creep*. Tertiary creep leads to the final rupture of the material and is associated with the evolution of internal damage. Internal damage will be discussed in Chapter 12. Prediction of creep behaviour is important, for instance, in situations where load-carrying metallic components are subjected to long duration loads at high temperatures. The need for consideration of creep response arises typically in the design and analysis of nuclear reactor and jet turbine engine components.

The third aspect of rate dependence, illustrated in Figure 11.1, is the phenomenon of stress *relaxation*. The graph of Figure 11.1(c) shows the typical evolution of stress in a relaxation test. The relaxation test consists of stretching the specimen (virtually instantaneously) to a prescribed axial strain and maintaining it strained (at constant strain) over a long period of time. The time-dependent response in this case is characterised by the continuous decay of stress in time. The prediction of stress relaxation can be vital, for instance, in the design of pre-stressed load-carrying components. We remark that the strain rate dependence of the stress response as well as the phenomena of creep and stress relaxation illustrated above for metals can also be observed for other materials by means of appropriate experiments.



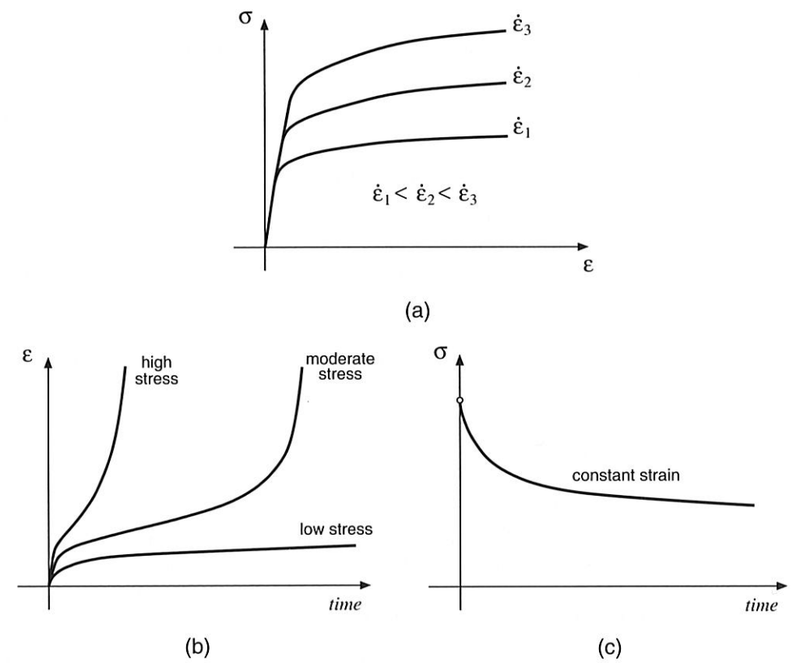


**Figure 11.1.** Viscoplasticity. Phenomenological aspects: uniaxial tensile tests at high temperature. (a) *Strain rate dependence*. Uniaxial tests at different strain rates. (b) *Creep*. Plastic flow at constant stress. (c) *Relaxation*. Stress decay at constant strain.

## 11.2. One-dimensional viscoplasticity model

Similarly to what has been done in Chapter 6 for rate-independent plasticity (refer to Section 6.2, from page 141), we find it convenient to introduce viscoplasticity by focusing first on a simple one-dimensional theory. Thus, we devote this section to the description of a simple uniaxial viscoplastic constitutive model. As we shall see, in spite of its simplicity, the uniaxial model possesses all the basic ingredients of the multidimensional models discussed in the remainder of this chapter. In particular, the model is able to capture many of the main features of the viscoplastic behaviour depicted in Figure 11.1.

### 11.2.1. ELASTOPLASTIC DECOMPOSITION OF THE AXIAL STRAIN

As for the rate-independent case, the decomposition of the total axial strain into a sum of an elastic (recoverable) and a plastic (permanent) component is introduced,

$$\varepsilon = \varepsilon^e + \varepsilon^p. \tag{11.1}$$

### 11.2.2. THE ELASTIC LAW

The axial stress is again assumed to be related to the elastic component of the axial strain by means of the standard linear elastic constitutive relation

$$\sigma = E\,\varepsilon^e. \tag{11.2}$$

### 11.2.3. THE YIELD FUNCTION AND THE ELASTIC DOMAIN

Here, the existence of an elastic domain for the stress within which the material behaviour is purely elastic is also experimentally observed in many cases.† Thus, analogously to the rate-independent model of Section 6.2, the elastic domain can be conveniently defined by means of a *yield function*

$$\Phi(\sigma, \sigma_y) = |\sigma| - \sigma_y, \tag{11.3}$$

where $\sigma_y$ is the yield stress. The elastic domain is defined as the set

$$\mathscr{E} = \{\sigma \mid \Phi(\sigma, \sigma_y) < 0\}, \tag{11.4}$$

so that the behaviour is purely elastic whenever $|\sigma| < \sigma_y$.

### 11.2.4. VISCOPLASTIC FLOW RULE

The crucial difference between the uniaxial elastoplastic model of Section 6.2 and the viscoplasticity model introduced here lies in the definition of the flow rule, which describes the evolution of $\varepsilon^p$. The viscoplastic flow rule can be postulated with a format similar to that of the rate-independent case (see equation (6.10), page 144)

$$\dot{\varepsilon}^p = \dot{\gamma}(\sigma, \sigma_y)\,\mathrm{sign}(\sigma), \tag{11.5}$$

where sign is the *signum* function defined by (6.11).

In spite of its similarity to the rate-independent flow rule, the above constitutive equation for $\varepsilon^p$ differs fundamentally from (6.10). Firstly, it needs to be emphasised that in the rate-independent model the plastic strain rate is in fact a *pseudo*-time rate; that is, $\dot{\varepsilon}^p$ in the rate-independent theory is the derivative of the plastic strain in respect to a *pseudo*-time parameter used solely to describe the sequence of events. In that case, the actual timescale is irrelevant. In contrast, the plastic strain rate in (11.5) is the actual time derivative of $\varepsilon^p$. In addition to this conceptual difference, $\dot{\gamma}$ – named the plastic multiplier and determined by the procedure of Section 6.2.7 (page 146) in the rate-independent theory – is here a *given* explicit function of $\sigma$ and $\sigma_y$. Essentially, the explicit function for $\dot{\gamma}$ should model how the rate of plastic straining varies with the level of stress. Many forms are possible for $\dot{\gamma}$ and a discussion on this issue will be left for Section 11.3. Here, we will define the one-dimensional viscoplasticity model by adopting the following particular definition

$$\dot{\gamma}(\sigma, \sigma_y) = \begin{cases} \dfrac{1}{\mu}\left[\left(\dfrac{|\sigma|}{\sigma_y}\right)^{1/\epsilon} - 1\right] & \text{if } \Phi(\sigma, \sigma_y) \geq 0 \\ 0 & \text{if } \Phi(\sigma, \sigma_y) < 0, \end{cases} \tag{11.6}$$

†As we shall see later in this chapter, some models of viscoplasticity do not have an elastic domain. Such models do not require the definition of a yield function.



where the material constants are the *viscosity-related* parameter $\mu$, whose dimension is time, and the non-dimensional *rate-sensitivity* parameter, $\epsilon$. Both parameters are strictly positive. This particular form has been introduced by Perić (1993) similarly to the power law form of the viscoplastic potential proposed by Perzyna (1963). It is important to emphasise that the material parameters $\mu$ and $\epsilon$ are *temperature dependent*. As a general rule, as temperature increases (decreases) $\mu$ and $\epsilon$ increase (decrease). For many metals, $\mu, \epsilon \to 0$ for sufficiently low temperatures, when the material behaviour may be assumed rate-independent.

### 11.2.5. HARDENING LAW

In the rate-independent case, the phenomenon of hardening describes the changes in yield stress that result from plastic straining. In the viscoplastic model, hardening can be incorporated in the same manner as in the elastoplastic case by letting the yield stress, $\sigma_y$, be a given (experimentally determined) function

$$\sigma_y = \sigma_y(\bar{\varepsilon}^p) \tag{11.7}$$

of the accumulated plastic strain

$$\bar{\varepsilon}^p = \int_0^t |\dot{\varepsilon}^p|\,\mathrm{d}t. \tag{11.8}$$

Note that (11.6) implies that at a given constant applied stress $\sigma$, an increase (decrease) in $\sigma_y$ will produce a decrease (increase) in the plastic strain rate $\dot{\varepsilon}^p$. As in the elastoplastic case, an increase of $\sigma_y$ will be referred to as *hardening* whereas its reduction will be described as *softening*. If $\sigma_y$ is a constant, the model is referred to as *perfectly* viscoplastic.

### 11.2.6. SUMMARY OF THE MODEL

The overall one-dimensional viscoplasticity model is defined by the constinutive equations (11.1)–(11.8). For convenience we summarise the model in Box 11.1.

### 11.2.7. SOME SIMPLE ANALYTICAL SOLUTIONS

Section 11.1 discussed some of the phenomenological aspects of viscoplastic behaviour. One important aspect to be emphasised here is that, in spite of its simplicity, the above-defined one-dimensional model can capture the key phenomenological features of rate-dependent plasticity shown in Figure 11.1. To illustrate this and give the reader a better insight into the theory, we derive in this section analytical solutions for three simple problems where the basic properties of *creep* at constant stress, *strain rate dependence* of the stress response and *stress relaxation* under constant strain are reproduced by the one-dimensional model.

#### *Creeping at constant stress*

Let us consider the case of a bar subjected to an axial load that produces a uniform stress $\sigma > \sigma_y$ over its cross-section. The load is applied instantaneously and, after being applied, remains constant in time.

With the instantaneous loading (at time $t = 0$), the bar will initially deform (also instantaneously) in a purely elastic manner. The fact that the model behaviour is elastic under

**Box 11.1.** One-dimensional viscoplastic constitutive model.

1. Elastoplastic split of the axial strain

$$\varepsilon = \varepsilon^e + \varepsilon^p$$

2. Uniaxial elastic law

$$\sigma = E\,\varepsilon^e$$

3. Yield function

$$\Phi(\sigma, \sigma_y) = |\sigma| - \sigma_y$$

4. Plastic flow rule

$$\dot{\varepsilon}^p = \dot{\gamma}\ \text{sign}(\sigma)$$

$$\dot{\gamma} = \begin{cases} \dfrac{1}{\mu}\left[\left(\dfrac{|\sigma|}{\sigma_y}\right)^{1/\epsilon} - 1\right] & \text{if } \Phi(\sigma, \sigma_y) \geq 0 \\ 0 & \text{if } \Phi(\sigma, \sigma_y) < 0 \end{cases}$$

5. Hardening law

$$\sigma_y = \sigma_y(\bar{\varepsilon}^p)$$

$$\dot{\bar{\varepsilon}}^p = \dot{\gamma}$$

instantaneous loading is formally demonstrated in the next example when the strain rate dependence of the stress response is discussed. However, even without a formal proof, it makes sense to accept that, as there is no time for plastic strains to develop over an (idealised) instantaneous loading event, the behaviour must be purely elastic under such a condition. Assuming zero initial plastic strain, it follows from the elastoplastic split of the total strain together with the elastic law that the total strain in the bar at $t = 0$, immediately after the instantaneous application of load, will be

$$\varepsilon_0 = \varepsilon_0^e = \frac{\sigma}{E}, \tag{11.9}$$

where the zero subscript denotes quantities at $t = 0$. From this moment on, the bar is kept under a constant stress above the yield limit. Under constant stress, the elastic law implies that the elastic strain will also remain constant. Thus, the straining of the bar after the instantaneous loading will be due purely to viscoplastic flow and will be modelled by constitutive equations (11.5), (11.6). Assuming that $\sigma$ is positive (tensile), we then have

$$\dot{\varepsilon}^p = \frac{1}{\mu}\left[\left(\frac{\sigma}{\sigma_y}\right)^{1/\epsilon} - 1\right]. \tag{11.10}$$

For a perfectly viscoplastic material (constant $\sigma_y$), the integration of the above equation, in conjunction with the elastoplastic decomposition of the total strain and the initial condition (11.9), gives the following solution for the straining of the bar

$$\varepsilon(t) = \frac{\sigma}{E} + \frac{1}{\mu}\left[\left(\frac{\sigma}{\sigma_y}\right)^{1/\epsilon} - 1\right] t. \tag{11.11}$$



The creep rate in this case is constant and proportional to $(\sigma/\sigma_y)^{1/\epsilon} - 1$. The material constants ($\mu$ and $\epsilon$) could be calibrated, for instance, so as to capture the initial branches of the creep curves of the material (refer to Figure 11.1(b)). The initial branches describe the phenomenon of *primary creep*. A hardening law could be incorporated to include the follow-up of the curves to their second straight branch that describes secondary creep.

### *Strain-rate dependence of the stress response*

Here we analyse the monotonic stretching of an initially unstrained (and unstressed) bar at constant strain rates. These are the conditions typically encountered in conventional tensile tests. The objective here is to show that the one-dimensional model is capable of predicting the strain-rate dependence of the stress response as generally illustrated in Figure 11.1(a).

Before stating the associated initial value problem, let us first recall that the material response within the elastic domain ($\sigma < \sigma_y$) is purely elastic. Thus, at the initial stages of the monotonic stretching process, the stress response does not depend on the rate of stretching. The stress–strain response during this phase is expressed simply as

$$\sigma = E\,\varepsilon \quad \text{if} \quad \sigma < \sigma_y, \tag{11.12}$$

or, equivalently,

$$\sigma = E\,\varepsilon \quad \text{if} \quad \varepsilon < \varepsilon^*, \tag{11.13}$$

where $\varepsilon^*$ is the strain at which the yield stress is reached

$$\varepsilon^* = \frac{\sigma_y}{E}. \tag{11.14}$$

Viscoplastic flow (and rate-dependent behaviour) may only take place when $\sigma \geq \sigma_y$ or, in terms of the applied strain, when $\varepsilon \geq \varepsilon^*$. Then, as our purpose is to illustrate the rate dependence predicted by the model, our initial value problem will be defined only over the portion of the loading process where $\sigma \geq \sigma_y$ (or $\varepsilon \geq \varepsilon^*$). To simplify the problem, we will assume that the material is perfectly viscoplastic (constant $\sigma_y$) and, in addition, the rate sensitivity parameter will be set to

$$\epsilon = 1,$$

so that an analytical solution to the initial value problem can be easily found.

*The initial value problem.*

The evolution of the plastic strain for the present model is defined by equation (11.10). Under the above assumptions, the associated initial value problem consists of finding a function $\varepsilon^p(t)$ such that

$$\dot{\varepsilon}^p(t) = \frac{1}{\mu}\left[\frac{\sigma(t)}{\sigma_y} - 1\right] = \frac{1}{\mu}\left\{\frac{E\,[\varepsilon(t) - \varepsilon^p(t)]}{\sigma_y} - 1\right\} = \frac{1}{\mu}\left[\frac{\varepsilon(t) - \varepsilon^p(t)}{\varepsilon^*} - 1\right], \tag{11.15}$$

where the total strain is the prescribed function

$$\varepsilon(t) = \alpha\, t + \varepsilon^* = \alpha\, t + \frac{\sigma_y}{E}, \tag{11.16}$$

corresponding to monotonic stretching with arbitrary (constant) strain rate $\alpha \geq 0$. Note that $t = 0$ corresponds to the onset of viscoplastic flow ($\sigma = \sigma_y \Leftrightarrow \varepsilon = \varepsilon^*$). The initial condition for $\varepsilon^p$ (the plastic strain at the onset of viscoplastic flow) is obviously

$$\varepsilon^p(0) = 0. \tag{11.17}$$

*The analytical solution.*

By substituting (11.16) into the differential equation (11.15), the initial value problem can be written as

$$\dot{\varepsilon}^p(t) = \frac{1}{\mu\,\varepsilon^*}[\alpha\, t - \varepsilon^p(t)]; \quad \varepsilon^p(0) = 0. \tag{11.18}$$

The analytical solution can then be promptly obtained by standard methods for first-order ordinary linear differential equations as

$$\varepsilon^p(t) = \alpha\big[t - \mu\,\varepsilon^*\big(1 - \mathrm{e}^{\frac{-t}{\mu\,\varepsilon^*}}\big)\big]. \tag{11.19}$$

By placing the above solution together with (11.16) into the elastic law, $\sigma = E(\varepsilon - \varepsilon^p)$, we obtain, after a straightforward manipulation, the following solution for the stress as a function of time

$$\sigma(t) = \sigma_y\big[1 + \alpha\,\mu\big(1 - \mathrm{e}^{\frac{-t}{\mu\,\varepsilon^*}}\big)\big]. \tag{11.20}$$

*The stress–strain response.*

The strain rate dependence of the stress response can be more clearly illustrated by expressing the stress as a function of strain for an arbitrary (but constant in time) strain rate, so that curves such as those depicted in Figure 11.1(a) can be produced. In the present case, such a function can be obtained by means of a simple variable transformation in (11.20). Indeed, note that by inverting the function defined by (11.16), we have

$$t = t(\varepsilon) = \frac{\varepsilon - \varepsilon^*}{\alpha}. \tag{11.21}$$

With the introduction of this relation into (11.20), we obtain

$$\tilde{\sigma}(\varepsilon) = \sigma(t(\varepsilon)) = \sigma_y\big\{1 + \alpha\,\mu\big[1 - \mathrm{e}^{\frac{1}{\mu\,\alpha}(1 - \frac{\varepsilon}{\varepsilon^*})}\big]\big\}, \tag{11.22}$$

which gives the stress–strain curve for an arbitrary strain rate $\alpha$. Insight into the problem can be gained by looking into the limit stress–strain curves, i.e. the curves obtained at infinitely slow rates ($\alpha \to 0$) and infinitely fast processes ($\alpha \to \infty$). In order to obtain the limit for infinitely slow rates, we first observe that, in the present monotonic loading process, the term

$$1 - \varepsilon/\varepsilon^*$$

in (11.22) is always negative. In addition, $\mu$ and $\alpha$ are positive so that the last term on the right-hand side of (11.22) is the exponential of a negative number. The limit is then easily obtained as

$$\lim_{\alpha \to 0} \tilde{\sigma}(\varepsilon) = \sigma_y; \tag{11.23}$$



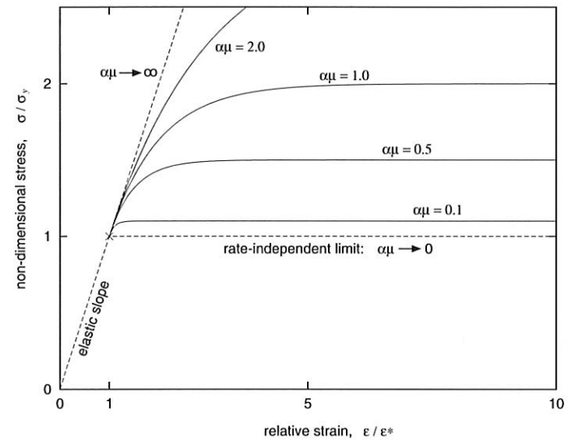


**Figure 11.2.** One-dimensional viscoplasticity model. Analytical solution showing the dependence of the stress response on the applied strain rate/viscosity parameter.

that is, at infinitely slow rates the perfectly viscoplastic model rigorously recovers the behaviour of the rate-independent plasticity model with yield stress $\sigma_y$. The rate-independent model was described in Section 6.2 (page 141). It is also very important to note that the same limit is obtained for the vanishing viscosity parameter, i.e. when $\mu \to 0$. At infinitely fast rates, the limit is derived by a standard limiting procedure which gives

$$\lim_{\alpha \to \infty} \tilde{\sigma}(\varepsilon) = E\,\varepsilon, \tag{11.24}$$

i.e. the process is purely elastic and the stress–strain curve after the yield limit is the continuation (with the same slope, $E$) of the elastic curve. Also note that the identical limit is found for $\mu \to \infty$ (infinitely viscous material). For any other rate (or viscosity parameter), the corresponding stress–strain curve will lie between these two limits with higher stress obtained at higher strain rates (or higher viscosity). To illustrate better the behaviour of the model under the present conditions, the analytical solution (11.22) is shown in the graph of Figure 11.2, where the non-dimensional stress, $\sigma/\sigma_y$, is plotted against the relative strain, $\varepsilon/\varepsilon^*$, for various normalised strain rates $\mu\alpha$. The limits $\mu\alpha \to 0$ (infinitely slow rates or non-viscous material) and $\mu\alpha \to \infty$ (infinitely fast rates or infinitely viscous material) are also included. Clearly, the model is able to capture the experimentally observed rate-dependence phenomenon illustrated in Figure 11.1(a).

**Remark 11.1.** In fact, even though it is not formally shown here, the above limits remain valid for any hardening curve and any rate sensitivity parameter $\epsilon$; that is, at infinitely slow strain rates, the model recovers the rate-independent behaviour of the plasticity model of Section 6.2 (this limit is also obtained for $\mu \to 0$) and, at infinitely fast rates (or when $\mu \to \infty$), the model behaves in a purely elastic manner, regardless of the given hardening curve and rate-sensitivity parameter. In addition (again not formally shown in this section), the

rate-independent behaviour is also recovered with vanishing rate-sensitivity, i.e. when $\epsilon \to 0$. This last property will be demonstrated in Section 11.4.3 in the context of the general multidimensional theory.

***Stress relaxation at constant strain***

In this final example, we consider the case of a bar which is instantaneously stretched (stretched at an infinitely fast strain rate) to a total strain $\varepsilon$ and then kept stretched indefinitely at that constant strain. The instantaneous stretching to $\varepsilon$ is assumed to produce a stress above the yield limit of the material. Here the model should be able to capture the phenomenon of stress relaxation alluded to in Figure 11.1(c).

Over the instantaneous stretching (at time $t = 0$), the bar will deform purely elastically (refer to the limit expression (11.24) and the text surrounding it). Thus, assuming that the plastic strain is zero at $t = 0$ (immediately after the instantaneous stretching), we have

$$\varepsilon_0^e = \varepsilon, \tag{11.25}$$

and, in view of the elastic law, the corresponding stress is given by

$$\sigma_0 = E\,\varepsilon_0^e = E\,\varepsilon. \tag{11.26}$$

From this point on, the stress in the bar will be governed by the law

$$\sigma = E(\varepsilon - \varepsilon^p) = \sigma_0 - E\,\varepsilon^p, \tag{11.27}$$

where $\varepsilon^p$ evolves in time according to the differential equation (11.10) which, in view of the above expression can be equivalently written as

$$\dot{\varepsilon}^p = \frac{1}{\mu}\left[\left(\frac{\sigma_0 - E\,\varepsilon^p}{\sigma_y}\right)^{1/\epsilon} - 1\right]. \tag{11.28}$$

To simplify the problem, we will assume, as in the previous example, that the material is perfectly viscoplastic (constant $\sigma_y$) and $\epsilon = 1$. In this case, the initial value problem is to find a function $\varepsilon^p(t)$ such that

$$\dot{\varepsilon}^p(t) = c_1 - c_2\,\varepsilon^p(t), \tag{11.29}$$

with initial condition

$$\varepsilon^p(0) = 0, \tag{11.30}$$

where the constants $c_1$ and $c_2$ are defined as

$$c_1 = \frac{1}{\mu}\left(\frac{\sigma_0}{\sigma_y} - 1\right), \quad c_2 = \frac{E}{\mu\,\sigma_y}. \tag{11.31}$$

The analytical solution to (11.29–11.30) can be trivially obtained as

$$\varepsilon^p(t) = \frac{c_1}{c_2}(1 - \mathrm{e}^{-c_2\,t}). \tag{11.32}$$



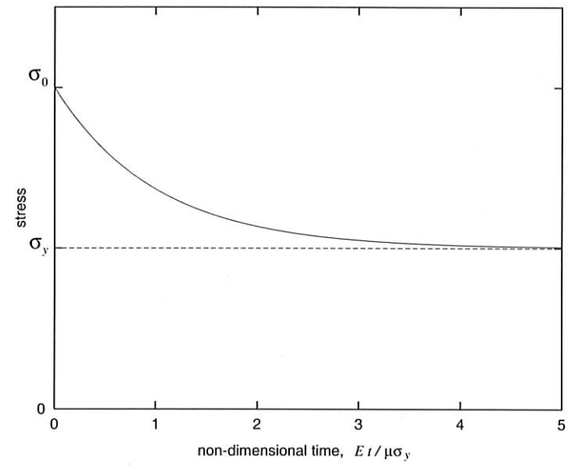


**Figure 11.3.** One-dimensional viscoplasticity model. Analytical solution to the stress relaxation problem.

Finally, by placing the above solution into (11.27), and taking into account the definition of $c_1$ and $c_2$, we obtain the stress as a function of time

$$\sigma(t) = \sigma_0 - (\sigma_0 - \sigma_y)(1 - \mathrm{e}^{-\frac{E}{\mu\,\sigma_y}t}). \tag{11.33}$$

Clearly, the above function describes the stress relaxation process of the bar, with the stress taking the value $\sigma = \sigma_0 > \sigma_y$ at $t = 0$ and subsequently relaxing asymptotically to $\sigma_y$ as $t \to \infty$. This is illustrated in Figure 11.3 where a graph of the analytical function $\sigma(t)$ (with $\sigma_0 = 2\,\sigma_y$) is plotted. The analytical solution with the present one-dimensional model clearly captures the experimentally observed behaviour referred to in Figure 11.1(c).

## 11.3. A von Mises-based multidimensional model

This section introduces a multidimensional extension of the one-dimensional model discussed above (and summarised in Box 11.1). Rather than define a generic extension at the outset (as in Section 6.3 (page 148) where a general multidimensional extension of the one-dimensional rate-independent plasticity model of Section 6.2 (page 141) was presented), we chose here to focus first on a von Mises-based generalisation of the uniaxial theory. A discussion of a more generic model, including its potential structure and its relation to time-independent plasticity as a limit case, will be left for Section 11.4.

### 11.3.1. A VON MISES-TYPE VISCOPLASTIC MODEL WITH ISOTROPIC STRAIN HARDENING

The multidimensional generalisation of the uniaxial viscoplastic model follows the same basic steps as the generalisation presented in Section 6.3 for the rate-independent theory;

**Box 11.2.** A von Mises-type viscoplastic constitutive model.

1. Elastoplastic split of the strain tensor

$$\boldsymbol{\varepsilon} = \boldsymbol{\varepsilon}^e + \boldsymbol{\varepsilon}^p$$

2. Linear elastic law

$$\boldsymbol{\sigma} = \mathbf{D}^e : \boldsymbol{\varepsilon}^e$$

3. Yield function

$$\Phi(\boldsymbol{\sigma}, \sigma_y) = q(\boldsymbol{s}(\boldsymbol{\sigma})) - \sigma_y; \quad q = \sqrt{\tfrac{3}{2}\, \boldsymbol{s} : \boldsymbol{s}}$$

and elastic domain

$$\mathscr{E} = \{\boldsymbol{\sigma} \mid \Phi(\boldsymbol{\sigma}, \sigma_y) < 0\}$$

4. Plastic flow rule

$$\dot{\boldsymbol{\varepsilon}}^p = \dot{\gamma}\, \frac{\partial \Phi}{\partial \boldsymbol{\sigma}} = \dot{\gamma} \sqrt{\frac{3}{2}}\, \frac{\boldsymbol{s}}{\|\boldsymbol{s}\|}$$

$$\dot{\gamma} = \begin{cases} \dfrac{1}{\mu}\left[\left(\dfrac{q}{\sigma_y}\right)^{1/\epsilon} - 1\right] & \text{if } \Phi(\boldsymbol{\sigma}, \sigma_y) \geq 0 \\ 0 & \text{if } \Phi(\boldsymbol{\sigma}, \sigma_y) < 0 \end{cases}$$

5. Isotropic strain hardening law

$$\sigma_y = \sigma_y(\bar{\varepsilon}^p); \quad \bar{\varepsilon}^p = \int_0^t \|\dot{\boldsymbol{\varepsilon}}^p\|\, \mathrm{d}t$$

6. Evolution of accumulated plastic strain

$$\dot{\bar{\varepsilon}}^p = \dot{\gamma}$$

that is, the elastoplastic split of the total strain, the linear elasticity law, the flow rule and yield function are recast in terms of the corresponding *tensor* quantities (total, elastic and plastic strain tensors, stress tensor and flow vector). The yield function is also redefined as a function of variables of appropriate tensorial order. The usual concept of an elastic domain bounded by a yield surface in the rate-independent theory will remain valid in the viscoplastic case. Here, as our multidimensional extension is von Mises-based, the yield function and the plastic flow rule (including the hardening internal variable) will have the same format as that of the standard rate-independent von Mises model with (associative) Prandtl–Reuss flow vector. The resulting model is a viscoplastic version of the rate-independent isotropically hardening von Mises model summarised in Section 7.3.1 (from page 216). The constitutive equations of the von Mises-based extension are listed in Box 11.2.

**Remark 11.2.** Analogously to its rate-independent counterpart, under uniaxial stress conditions, the model of Box 11.2 reduces exactly to the one-dimensional theory of Box 11.1. It is also important to emphasise that the basic properties of creep, stress relaxation and strain-rate dependence of the stress response (including the behaviour at limits) as demonstrated for the



uniaxial model in Section 11.2.7 are reproduced by the multidimensional theory under any state of stress.

### 11.3.2. ALTERNATIVE PLASTIC STRAIN RATE DEFINITIONS

So far, the explicit function for $\dot{\gamma}$ that takes part in the definition of the plastic flow equation (see expression (11.6) and item 4 of Boxes 11.1 and 11.2) has been assumed to be of the form proposed by Perić (1993). As mentioned in Section 11.2.4, many forms for $\dot{\gamma}$ have been proposed and, in practice, a particular choice should be dictated by its ability to model the dependence of the plastic strain rate on the state of stress for the material under consideration. In this section, we list some of the most widely used forms. Clearly, each form of $\dot{\gamma}$ defines a different model of viscoplasticity. However, within the framework of von Mises viscoplasticity, the format of the flow rule

$$\dot{\boldsymbol{\varepsilon}}^p = \dot{\gamma}\, \boldsymbol{N}, \tag{11.34}$$

with associative flow vector $\boldsymbol{N}$ defined by

$$\boldsymbol{N} = \frac{\partial \Phi}{\partial \boldsymbol{\sigma}} = \sqrt{\frac{3}{2}}\, \frac{\boldsymbol{s}}{\|\boldsymbol{s}\|}, \tag{11.35}$$

and yield function

$$\Phi(\boldsymbol{\sigma}, \sigma_y) = q(\boldsymbol{s}(\boldsymbol{\sigma})) - \sigma_y, \tag{11.36}$$

will remain unchanged for any definition of $\dot{\gamma}$.

#### *Bingham model*

The Bingham model is the simplest model of viscoplasticity. The multiplier $\dot{\gamma}$ in this case is defined as

$$\dot{\gamma}(\boldsymbol{\sigma}, \sigma_y) = \begin{cases} \dfrac{1}{\eta}\, \Phi(\boldsymbol{\sigma}, \sigma_y) = \dfrac{q(\boldsymbol{\sigma}) - \sigma_y}{\eta} & \text{if } \Phi(\boldsymbol{\sigma}, \sigma_y) \geq 0 \\ 0 & \text{if } \Phi(\boldsymbol{\sigma}, \sigma_y) < 0. \end{cases} \tag{11.37}$$

The only material constant in this case is the (temperature-dependent) viscosity parameter $\eta$ and the strain rate is modelled as a *linear* function of the von Mises effective stress. Note that this law is obtained from Perić's model given in item 4 of Box 11.2 (and also from the Perzyna model described below) by setting

$$\epsilon = 1; \quad \mu = \frac{\eta}{\sigma_y}. \tag{11.38}$$

In the uniaxial case, the plastic strain rate for the Bingham model is a linear function of the axial stress:

$$\dot{\varepsilon}^p = \frac{1}{\eta}\, (|\sigma| - \sigma_y)\, \mathrm{sign}(\sigma). \tag{11.39}$$

This may severely limit the ability of the model to fit experimental data as, in many cases, the observed strain rate may be a markedly nonlinear function of the stress. However, over a relatively narrow range of stresses, the linear approximation may give good results. Other models, with more material constants, have, in general, better flexibility to allow a wider range of experimental data to be fitted.

***Perzyna model***

This model was introduced by Perzyna (1966, 1971) and is widely used in computational applications of viscoplasticity. It is defined by

$$\dot{\gamma}(\boldsymbol{\sigma}, \sigma_y) = \begin{cases} \dfrac{1}{\mu}\left[\dfrac{q(\boldsymbol{\sigma})}{\sigma_y} - 1\right]^{1/\epsilon} & \text{if } \Phi(\boldsymbol{\sigma}, \sigma_y) \geq 0 \\ 0 & \text{if } \Phi(\boldsymbol{\sigma}, \sigma_y) < 0. \end{cases} \tag{11.40}$$

As in Perić's model, the material constants are the viscosity-related parameter, $\mu$, and the rate sensitivity, $\epsilon$. We remark here that, in spite of its similarity to Perić's definition, as the rate-independent limit is approached with vanishing rate-sensitivity $\epsilon \to 0$ (refer to Remark 11.1 on page 443), the Perzyna model does not reproduce the uniaxial stress–strain curve of the corresponding rate-independent model with yield stress $\sigma_y$. As shown by Perić (1993), in this limit, the Perzyna model produces a curve with $\sigma = 2\,\sigma_y$ instead. However, for vanishing viscosity ($\mu \to 0$) or vanishing strain rates, the response of both Perzyna and Perić models coincide with the standard rate-independent model with yield stress $\sigma_y$.

### 11.3.3. OTHER ISOTROPIC AND KINEMATIC HARDENING LAWS

In the viscoplasticity model of Box 11.2, only isotropic strain hardening has been taken into account. Other hardening laws, such as isotropic work hardening (where the plastic work is taken as the internal variable) as well as kinematic hardening and more general mixed isotropic/kinematic hardening rules can be considered in a manner completely analogous to that of the rate-independent theory as described in Section 6.6 (page 177); that is, isotropic work hardening is obtained by having $\sigma_y$ as a given function of the plastic work, $w^p$, defined by expression (6.177)

$$\sigma_y = \sigma_y(w^p). \tag{11.41}$$

Kinematic hardening is introduced by simply replacing the von Mises effective stress, $q$, with the *relative* effective stress

$$\bar{q} = \sqrt{\tfrac{3}{2}\,\boldsymbol{\eta} : \boldsymbol{\eta}}, \tag{11.42}$$

where $\boldsymbol{\eta}$ is the relative stress

$$\boldsymbol{\eta} = \boldsymbol{s} - \boldsymbol{\beta}, \tag{11.43}$$

and $\boldsymbol{\beta}$ is the backstress tensor. Evolution laws for $\boldsymbol{\beta}$, such as Prager's rule and the Armstrong–Frederick kinematic hardening law, can be defined as in Section 6.6.

### 11.3.4. VISCOPLASTIC MODELS WITHOUT A YIELD SURFACE

The assumption of the existence of an elastic domain bounded by a yield surface is essential in the formulation of rate-independent plasticity models. For viscoplasticity models, however, such an assumption is by no means required. In fact, particularly at higher temperatures, many materials can be modelled as flowing whenever under stress; that is, the yield stress is effectively zero. For example, many metals at high temperatures will flow at virtually any stress state with a non-zero deviatoric component. In such cases, a yield surface and a corresponding elastic domain do not need to be introduced in the formulation of the



theory. Viscoplasticity models without a yield surface have been used widely, especially in the analysis of creep and hot metal forming operations. Within the present framework, such models can be defined simply by postulating the explicit function for $\dot{\gamma}$ accordingly.

***Norton's creep law***

The classical Norton creep law has been employed extensively in the analysis of creep of metals. It is used mainly in the description of secondary creep. In its original (uniaxial) version, the flow rule is given by

$$\dot{\varepsilon}^p = \left(\frac{|\sigma|}{\lambda}\right)^N \operatorname{sign}(\sigma), \tag{11.44}$$

where $N$ and $\lambda$ are temperature-dependent material constants. Clearly, plastic flow is assumed to occur whenever $\sigma \neq 0$. Its multidimensional generalisation, sometimes referred to as Odqvist's law, is obtained by simply replacing the definition of the function for $\dot{\gamma}$ in item 4 of Box 11.2 with the following

$$\dot{\gamma}(\boldsymbol{\sigma}) = \left[\frac{q(\boldsymbol{\sigma})}{\lambda}\right]^N. \tag{11.45}$$

Here, plastic flow takes place for any stress with non-zero deviator. Note that, by setting $\sigma_y = 0$ in (11.37) the Bingham model recovers the Norton law with $N = 1$ and $\lambda = \eta$.

***Lemaitre–Chaboche law***

A modification of Norton's law in order to improve its ability to model secondary creep over a wider range of stresses and strain rates is provided by the Lemaitre–Chaboche law (Lemaitre and Chaboche, 1990). The function $\dot{\gamma}$ in this case reads

$$\dot{\gamma}(\boldsymbol{\sigma}) = \left[\frac{q(\boldsymbol{\sigma})}{\lambda}\right]^N \exp[\alpha\, q(\boldsymbol{\sigma})^{N+1}]. \tag{11.46}$$

In addition to the material parameters $N$ and $\lambda$ required by Norton's law, the present model has a third (also temperature-dependent) parameter $\alpha$.

***Other creep laws***

A rather general class of viscoplastic laws can be obtained by assuming that $\dot{\gamma}$ is a function of the stress, time and temperature, with the following multiplicative format

$$\dot{\gamma} = \dot{\gamma}(\boldsymbol{\sigma}, t, T) = f_\sigma(\boldsymbol{\sigma})\, f_t(t)\, f_T(T), \tag{11.47}$$

where $t$ and $T$ denote, respectively, the time and absolute temperature and $f_\sigma$, $f_t$ and $f_T$ are experimentally defined functions. A comprehensive list of proposed empirical functions is given by Skrzypek (1993), to which the interested reader is referred. For instance, $f_\sigma$ could be Norton's law or the Lemaitre–Chaboche relation above. The temperature function $f_T$ is

normally defined by the Arrhenius law

$$f_T(T) = C \exp\left[\frac{-Q}{RT}\right] \tag{11.48}$$

where $C$ is a constant, $Q$ is the *activation energy* usually independent of the temperature, $R$ is the gas constant 8.31 J mol$^{-1}$ $K^{-1}$. A typical example of an empirical relation of the above format is given by the law (Boyle and Spence, 1983)

$$\dot{\gamma} = C \exp\left[\frac{-Q}{RT}\right] t^M \, q^N, \tag{11.49}$$

with $M$ and $N$ being material parameters.

Another interesting viscoplastic model used primarily in the description of the behaviour of metallic alloys at high temperatures is the *Bodner–Partom* model (Bodner and Partom, 1975). An implicit computational implementation of the Bodner–Partom model has been recently described by Anderson (2003).

## 11.4. General viscoplastic constitutive model

Having described in the previous section some of the most commonly used viscoplasticity models, we proceed here to formulate a more general constitutive theory of viscoplasticity. The theory presented here is a viscoplastic version of the general rate-independent model described in Section 6.3 (from page 148) and summarised in Box 6.2 (page 151). At this point, note that we will use here the notation of Section 6.3. The reader who is not familiar with that notation, or concepts used in that section, is advised to review them before proceeding further. The formulation of the viscoplastic model is analogous to that of its rate-independent counterpart. It follows the same considerations as Sections 6.3.1 to 6.3.4, except that the flow rule and hardening law are defined as

$$\begin{aligned} \dot{\boldsymbol{\varepsilon}}^p &= \boldsymbol{G}(\boldsymbol{\sigma}, \boldsymbol{A}) \\ \dot{\boldsymbol{\alpha}} &= \boldsymbol{J}(\boldsymbol{\sigma}, \boldsymbol{A}); \end{aligned} \tag{11.50}$$

that is, the plastic strain rate and the evolution law for the set $\boldsymbol{\alpha}$ of hardening internal variables are defined by means of the *explicit* constitutive functions $\boldsymbol{G}$ and $\boldsymbol{J}$ of $\boldsymbol{\sigma}$ and the set $\boldsymbol{A}$ of hardening thermodynamic forces. In addition, as we have seen above, an elastic domain may not exist. Thus, a yield function is not necessarily present in the viscoplastic formulation. The constitutive equations of the general viscoplasticity model are listed in Box 11.3.

Note that the von Mises-based model of Box 11.2 (which incorporates an elastic domain) is trivially recovered by defining the functions $\boldsymbol{G}$ and $\boldsymbol{J}$ as well as the free-energy potential $\psi$ and the internal variable set $\boldsymbol{\alpha}$ accordingly. The same applies to all other models (with or without an elastic domain) described in Section 11.3.

### 11.4.1. RELATION TO THE GENERAL CONTINUUM CONSTITUTIVE THEORY

The above viscoplasticity model fits within the generic internal variable-based constitutive framework discussed in Section 3.5.2 (from page 71). Indeed, it can be trivially established



**Box 11.3.** A general viscoplastic constitutive model.

1. Additive decomposition of the strain tensor
$$\boldsymbol{\varepsilon} = \boldsymbol{\varepsilon}^e + \boldsymbol{\varepsilon}^p$$
2. Free-energy function
$$\psi = \psi(\boldsymbol{\varepsilon}^e, \boldsymbol{\alpha})$$
where $\boldsymbol{\alpha}$ is a set of hardening internal variables
3. Constitutive equation for $\boldsymbol{\sigma}$ and hardening thermodynamic forces $\boldsymbol{A}$
$$\boldsymbol{\sigma} = \bar{\rho}\,\frac{\partial \psi}{\partial \boldsymbol{\varepsilon}^e} \quad \boldsymbol{A} = \bar{\rho}\,\frac{\partial \psi}{\partial \boldsymbol{\alpha}}$$
4. Plastic flow rule and hardening law
$$\dot{\boldsymbol{\varepsilon}}^p = \boldsymbol{G}(\boldsymbol{\sigma}, \boldsymbol{A})$$
$$\dot{\boldsymbol{\alpha}} = \boldsymbol{J}(\boldsymbol{\sigma}, \boldsymbol{A})$$

that the model of Box 11.3 is a particular case of the general purely mechanical infinitesimal constitutive law defined by (3.165) on page 76. The general viscoplasticity model is obtained by simply defining the set $\boldsymbol{\alpha}$ of (3.165) as composed of the plastic strain tensor and the set of hardening internal variables (as described in Section 6.3.2) and then introducing the explicit constitutive functions for the rates of plastic strain and hardening variables listed in item 4 of Box 11.3.

### 11.4.2. POTENTIAL STRUCTURE AND DISSIPATION INEQUALITY

A specialisation of the general theory of Box 11.3 can be obtained by endowing the model with a potential structure (refer to the discussion surrounding expression (3.162) on page 74). In this case, we define a *dissipation potential*

$$\Xi = \Xi(\boldsymbol{\sigma}, \boldsymbol{A}), \tag{11.51}$$

from which, through the hypothesis of *normal dissipativity*, the evolution of the internal variables of the problem are derived as

$$\begin{aligned} \dot{\boldsymbol{\varepsilon}}^p &= \frac{\partial \Xi}{\partial \boldsymbol{\sigma}} \\ \dot{\boldsymbol{\alpha}} &= -\frac{\partial \Xi}{\partial \boldsymbol{A}}. \end{aligned} \tag{11.52}$$

At this point, it is important to recall that the *plastic dissipation* in the present case is given by (again, refer to Section 6.3.2)

$$\boldsymbol{\sigma} : \dot{\boldsymbol{\varepsilon}}^p - \boldsymbol{A} * \dot{\boldsymbol{\alpha}},$$

so that the dissipation inequality reads

$$\Upsilon^p(\boldsymbol{\sigma}, \boldsymbol{A}; \dot{\boldsymbol{\varepsilon}}^p, \dot{\boldsymbol{\alpha}}) \geq 0, \tag{11.53}$$

where

$$\Upsilon^p(\boldsymbol{\sigma}, \boldsymbol{A}; \dot{\boldsymbol{\varepsilon}}^p, \dot{\boldsymbol{\alpha}}) \equiv \boldsymbol{\sigma} : \dot{\boldsymbol{\varepsilon}}^p - \boldsymbol{A} * \dot{\boldsymbol{\alpha}} \tag{11.54}$$

is the *dissipation function*.

By defining $\Xi$ such that it is convex with respect to both variables, non-negative and zero-valued at $\{\boldsymbol{\sigma}, \boldsymbol{A}\} = \{\mathbf{0}, \mathbf{0}\}$ it is ensured that the dissipation inequality is satisfied *a priori* by the model.

### 11.4.3. RATE-INDEPENDENT PLASTICITY AS A LIMIT CASE

In this section we show that rate-independent plasticity can be recovered as a limit case of the above general viscoplastic theory with a potential structure. As emphasised above, the general viscoplastic model is a particular instance of the internal variable-based constitutive framework of Section 3.5.2. Thus, the demonstration that follows here shows effectively that, as anticipated in Section 6.3.7, the elastoplastic model of Box 6.3 (page 151) can be rigorously described, under some circumstances, as a particular case of the general continuum constitutive theory of Section 3.5.2.

#### *The indicator function of a convex set*

The demonstration presented here is based on arguments of convex analysis.[‡] Crucial to the proof to be shown is the concept of *indicator function* of a convex set. In this context, let us consider the closure, $\mathscr{A}$, of the elastic domain defined by means of a yield function $\Phi$:

$$\mathscr{A} = \{(\boldsymbol{\sigma}, \boldsymbol{A}) \mid \Phi(\boldsymbol{\sigma}, \boldsymbol{A}) \leq 0\}. \tag{11.55}$$

In rate-independent plasticity, $\mathscr{A}$ is the set of all *admissible* states $(\boldsymbol{\sigma}, \boldsymbol{A})$ of stress and hardening thermodynamical forces. The set $\mathscr{A}$ is *convex*, i.e. it defines a convex region in the space of stresses and hardening forces. Following the above considerations, we now introduce the *indicator function*, $\Psi_{\mathscr{A}}$, of the convex set $\mathscr{A}$ as the scalar-valued function defined by

$$\Psi_{\mathscr{A}}(\boldsymbol{\sigma}, \boldsymbol{A}) = \begin{cases} 0 & \text{if } (\boldsymbol{\sigma}, \boldsymbol{A}) \in \mathscr{A} \\ \\ \infty & \text{if } (\boldsymbol{\sigma}, \boldsymbol{A}) \notin \mathscr{A}. \end{cases} \tag{11.56}$$

The indicator function is clearly *non-differentiable*.

#### *The rate-independent limit*

In what follows, we shall see that an associative rate-independent plasticity model is obtained by adopting $\Psi_{\mathscr{A}}$ as the dissipation potential in the general viscoplastic theory; that is, we choose

$$\Xi(\boldsymbol{\sigma}, \boldsymbol{A}) \equiv \Psi_{\mathscr{A}}(\boldsymbol{\sigma}, \boldsymbol{A}). \tag{11.57}$$

[‡]Readers not familiar with convex analysis are referred to Rockafellar (1970).



At this point we need to make use of the concept of *subdifferential*.[§] In view of the non-differentiability of the indicator function, the constitutive equations (11.52), which follow from normal dissipativity, are replaced with the *subdifferential* relations

$$\begin{aligned} \dot{\boldsymbol{\varepsilon}}^p &\in \partial_{\boldsymbol{\sigma}} \Psi_{\mathscr{A}} \\ \dot{\boldsymbol{\alpha}} &\in -\partial_{\boldsymbol{A}} \Psi_{\mathscr{A}}, \end{aligned} \tag{11.58}$$

where $\partial_{\boldsymbol{\sigma}} \Psi_{\mathscr{A}}$ and $\partial_{\boldsymbol{A}} \Psi_{\mathscr{A}}$ are the subdifferentials of $\Psi_{\mathscr{A}}$ with respect to $\boldsymbol{\sigma}$ and $\boldsymbol{A}$, respectively. From the subdifferential definition (6.69) together with (11.56) it can easily be established that (11.58) is equivalent to the inequality

$$\dot{\boldsymbol{\varepsilon}}^p : (\boldsymbol{\sigma} - \boldsymbol{\sigma}^*) + \dot{\boldsymbol{\alpha}} * (\boldsymbol{A} - \boldsymbol{A}^*) \geq 0, \quad \forall\, (\boldsymbol{\sigma}^*, \boldsymbol{A}^*) \in \Psi_{\mathscr{A}}, \tag{11.59}$$

or, equivalently, in terms of the dissipation function (11.54)

$$\Upsilon^p(\boldsymbol{\sigma}, \boldsymbol{A}; \dot{\boldsymbol{\varepsilon}}^p, \dot{\boldsymbol{\alpha}}) \geq \Upsilon^p(\boldsymbol{\sigma}^*, \boldsymbol{A}^*; \dot{\boldsymbol{\varepsilon}}^p, \dot{\boldsymbol{\alpha}}), \quad \forall\, (\boldsymbol{\sigma}^*, \boldsymbol{A}^*) \in \mathscr{A}. \tag{11.60}$$

This last inequality states that, among all states $(\boldsymbol{\sigma}^*, \boldsymbol{A}^*) \in \mathscr{A}$, the actual stress and hardening force $(\boldsymbol{\sigma}, \boldsymbol{A})$ maximise the dissipation function. This is known as the *principle of maximum plastic dissipation*, discussed in Section 6.5.2 (page 170) to which the reader is referred for details. The solution to the maximisation problem associated with the principle of maximum plastic dissipation is the classical associative laws

$$\begin{aligned} \dot{\boldsymbol{\varepsilon}}^p &= \dot{\gamma}\, \frac{\partial \Phi}{\partial \boldsymbol{\sigma}} \\ \dot{\boldsymbol{\alpha}} &= -\dot{\gamma}\, \frac{\partial \Phi}{\partial \boldsymbol{A}}, \end{aligned} \tag{11.61}$$

together with the loading/unloading conditions of rate-independent plasticity

$$\Phi(\boldsymbol{\sigma}, \boldsymbol{A}) \leq 0, \quad \dot{\gamma} \geq 0, \quad \Phi(\boldsymbol{\sigma}, \boldsymbol{A})\dot{\gamma} = 0. \tag{11.62}$$

In summary, it has been shown above that the classical rate-independent associative plasticity equations are rigorously recovered from the general viscoplasticity model when the indicator function of the set $\mathscr{A}$ is taken as the dissipation potential.

#### *Example: von Mises-based model*

Let us now consider the von Mises-based model of Box 11.2 and, for simplicity, assume that the model is perfectly viscoplastic (constant $\sigma_y$). Our purpose here is to illustrate the above ideas by demonstrating that the viscoplastic model can be defined in terms of a dissipation potential whose limit when $\epsilon \to 0$ or $\mu \to 0$ is the indicator function of the set of admissible stresses of the perfectly plastic von Mises model. Thus, in such limits, the perfectly viscoplastic model rigorously recovers the classical perfectly elastoplastic von Mises model.

[§]Refer to Section 6.3.9 (from page 153) for the definition of subdifferential.

We start by defining the dissipation potential as

$$\Xi(\boldsymbol{\sigma}) = \begin{cases} \dfrac{\sigma_y}{\mu}\left\{\dfrac{1}{1+\epsilon} + \dfrac{\epsilon}{1+\epsilon}\left[\dfrac{q(\boldsymbol{\sigma})}{\sigma_y}\right]^{\frac{1+\epsilon}{\epsilon}} - \dfrac{q(\boldsymbol{\sigma})}{\sigma_y}\right\} & \text{if } q/\sigma_y \geq 1 \\ 0 & \text{if } q/\sigma_y < 1, \end{cases} \tag{11.63}$$

where $\boldsymbol{\sigma}$ is the only variable. With the above definition, the flow rule

$$\dot{\boldsymbol{\varepsilon}}^p = \frac{\partial \Xi}{\partial \boldsymbol{\sigma}}, \tag{11.64}$$

is found through a straightforward differentiation to be that of item 4 of Box 11.2; that is, the above potential indeed defines the von Mises-based viscoplasticity model of Box 11.2 when hardening is not considered.

Finally, by simple inspection, we can easily see that, when $\epsilon \to 0$ or $\mu \to 0$, the limit of the potential $\Xi$ of (11.63) is the indicator function of the set of admissible stresses defined by the von Mises yield function:

$$\lim_{\epsilon \to 0} \Xi(\boldsymbol{\sigma}) = \lim_{\mu \to 0} \Xi(\boldsymbol{\sigma}) = \Psi_{\mathscr{A}}(\boldsymbol{\sigma}), \tag{11.65}$$

where

$$\mathscr{A} = \{\boldsymbol{\sigma} \mid q(\boldsymbol{\sigma}) - \sigma_y \leq 0\}. \tag{11.66}$$

This completes the demonstration. The schematic illustration of Figure 11.4 shows the potential $\Xi$ for various choices of the rate-sensitivity parameter $\epsilon$. Clearly, as $\epsilon \to 0$, $\Xi$ tends to the indicator function of $\mathscr{A}$.

## 11.5. General numerical framework

This section describes the basic ingredients needed to incorporate the general viscoplasticity model of Box 11.3 into the finite element framework of Chapter 4. The basic requirements are:

(i) an algorithm for numerical integration of the viscoplastic constitutive equations, to be used to update stresses and other state variables of the model;

(ii) the associated consistent tangent modulus, to be used in the assemblage of the finite element stiffness matrix.

For further discussions and analysis of various aspects of the numerical treatment of viscoplasticity, we refer to Simo and Govindjee (1991), Perić (1993), Chaboche and Cailletaud (1996), Simo and Hughes (1998), Simo (1998), Runesson and Mahler (1999), and Alfano and Rosati (2001).

### 11.5.1. A GENERAL IMPLICIT INTEGRATION ALGORITHM

Before proceeding to the derivation of an integration algorithm for the general viscoplastic model, it seems convenient, for the sake of clarity, to start by stating the underlying initial value problem we wish to solve. The problem here is analogous to its rate-independent counterpart, Problem 7.1, stated on page 193.



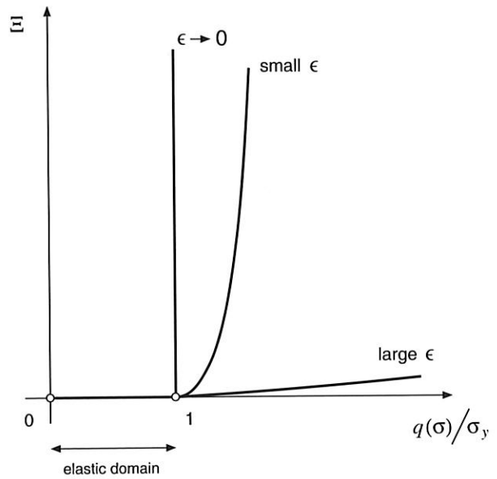


**Figure 11.4.** Viscoplastic potential $\Xi$ for various rate-sensitivity parameters $\epsilon$.

**Problem 11.1 (The viscoplastic constitutive initial value problem).** *Given the initial values $\boldsymbol{\varepsilon}^e(t_0)$ and $\boldsymbol{\alpha}(t_0)$ and given the history of the strain tensor, $\boldsymbol{\varepsilon}(t)$, $t \in [t_0, T]$, find the functions $\boldsymbol{\varepsilon}^e(t)$ and $\boldsymbol{\alpha}(t)$, for the elastic strain tensor and hardening internal variable set that satisfy the reduced general viscoplastic constitutive equations*

$$\dot{\boldsymbol{\varepsilon}}^e(t) = \dot{\boldsymbol{\varepsilon}}(t) - \boldsymbol{G}(\boldsymbol{\sigma}(t), \boldsymbol{A}(t)), \quad \dot{\boldsymbol{\alpha}}(t) = \boldsymbol{J}(\boldsymbol{\sigma}(t), \boldsymbol{A}(t)) \tag{11.67}$$

*for each instant $t \in [t_0, T]$, with*

$$\boldsymbol{\sigma}(t) = \bar{\rho}\left.\frac{\partial \psi}{\partial \boldsymbol{\varepsilon}^e}\right|_t, \quad \boldsymbol{A}(t) = \bar{\rho}\left.\frac{\partial \psi}{\partial \boldsymbol{\alpha}}\right|_t. \tag{11.68}$$

As in the definition of the rate-independent problem, the reduced system (11.67) of ordinary differential equations has been obtained by incorporating the viscoplastic flow equation $(11.50)_1$ into the elastoplastic split of the total strain rate so that the plastic strain does not appear explicitly in the initial value problem. Clearly, once the history of elastic strain is determined in the solution to the above problem, the history of the plastic strain is promptly obtained as

$$\boldsymbol{\varepsilon}^p(t) = \boldsymbol{\varepsilon}(t) - \boldsymbol{\varepsilon}^e(t). \tag{11.69}$$

The fully implicit algorithm for the numerical solution of the above problem is derived by simply applying a standard backward Euler time discretisation of the rate equations. The resulting incremental problem is presented in Box 11.4, where a typical step over the time interval $[t_n, t_{n+1}]$ is considered. The time and strain increments are defined in the usual way as

$$\Delta t = t_{n+1} - t_n, \quad \Delta \boldsymbol{\varepsilon} = \boldsymbol{\varepsilon}_{n+1} - \boldsymbol{\varepsilon}_n. \tag{11.70}$$

**Box 11.4.** Fully implicit algorithm for numerical integration of general viscoplastic constitutive equations.

Given the strain and time increment, $\Delta\boldsymbol{\varepsilon}$ and $\Delta t$, over $[t_n, t_{n+1}]$ and the state variables at $t_n$, compute the updated state by solving the nonlinear system of equations

$$\left\{\begin{array}{c} \boldsymbol{\varepsilon}^e_{n+1} - \boldsymbol{\varepsilon}^e_n - \Delta\boldsymbol{\varepsilon} + \Delta t\, \boldsymbol{G}(\boldsymbol{\sigma}_{n+1}, \boldsymbol{A}_{n+1}) \\ \boldsymbol{\alpha}_{n+1} - \boldsymbol{\alpha}_n - \Delta t\, \boldsymbol{J}(\boldsymbol{\sigma}_{n+1}, \boldsymbol{A}_{n+1}) \end{array}\right\} = \left\{\begin{array}{c} \mathbf{0} \\ \mathbf{0} \end{array}\right\}$$

for $\boldsymbol{\varepsilon}^e_{n+1}$ and $\boldsymbol{\alpha}_{n+1}$, with

$$\boldsymbol{\sigma}_{n+1} = \bar{\rho}\, \frac{\partial \psi}{\partial \boldsymbol{\varepsilon}^e}\bigg|_{n+1}, \quad \boldsymbol{A}_{n+1} = \bar{\rho}\, \frac{\partial \psi}{\partial \boldsymbol{\alpha}}\bigg|_{n+1}$$

### *Models with a yield surface*

Note that in the algorithm of Box 11.4 no assumption is made on the existence of an elastic domain. The algorithm is valid for models with or without a yield surface. If a yield surface is present, however, the specialisation of the algorithm of Box 11.4 takes a two-stage format completely analogous to the elastic predictor/return-mapping procedure of the rate-independent case. To see this, let us first consider that for a general model with a yield surface, the constitutive functions $\boldsymbol{G}$ and $\boldsymbol{J}$ can be defined with the following form

$$\begin{aligned} \boldsymbol{G}(\boldsymbol{\sigma}, \boldsymbol{A}) &= \dot{\gamma}(\boldsymbol{\sigma}, \boldsymbol{A})\, \boldsymbol{N}(\boldsymbol{\sigma}, \boldsymbol{A}) \\ \boldsymbol{J}(\boldsymbol{\sigma}, \boldsymbol{A}) &= \dot{\gamma}(\boldsymbol{\sigma}, \boldsymbol{A})\, \boldsymbol{H}(\boldsymbol{\sigma}, \boldsymbol{A}), \end{aligned} \tag{11.71}$$

where, following the terminology of the rate-independent theory, $\boldsymbol{N}$ is the flow vector and $\boldsymbol{H}$ is the generalised hardening modulus. The scalar $\dot{\gamma}$ is zero within the elastic domain or on the yield surface and may only be non-zero outside the elastic domain. Clearly, evolution of $\boldsymbol{\varepsilon}^p$ and $\boldsymbol{\alpha}$ may only occur here at states with $\Phi(\boldsymbol{\sigma}, \boldsymbol{A}) > 0$, i.e. states lying neither in the elastic domain nor on the yield surface. Then, as in the rate-independent case, it makes sense to first compute an *elastic trial state* by assuming that the material behaviour is purely elastic within the interval $[t_n, t_{n+1}]$. If the trial state is within the elastic domain or on the yield surface, then no viscoplastic flow takes place within the considered time step and the trial state is the actual state at the end of the step. Otherwise, the evolution of $\boldsymbol{\varepsilon}^p$ and $\boldsymbol{\alpha}$ is computed by means of the standard backward Euler method. The resulting algorithm, which we shall refer to as the *elastic predictor/viscoplastic corrector* or *elastic predictor/viscoplastic return mapping* algorithm, is listed in Box 11.5.

**Remark 11.3.** The viscoplastic return mapping differs from its elastoplastic (rate-independent) counterpart (refer to Box 7.1, page 199) in that, here, the updated stress state at $t_{n+1}$ generally lies on the outside of the yield surface, i.e.

$$\Phi(\boldsymbol{\sigma}_{n+1}, \boldsymbol{A}_{n+1}) > 0.$$

This is in contrast with the rate-independent case in which the consistency equation, $\Phi_{n+1} = 0$, forces the updated state to be on the yield surface when there is plastic flow over



**Box 11.5.** Fully implicit elastic predictor/viscoplastic return-mapping algorithm for numerical integration of general viscoplastic constitutive equations with a yield surface over a generic time interval $[t_n, t_{n+1}]$ with $\Delta t = t_{n+1} - t_n$.

(i) Elastic predictor. Given $\Delta\boldsymbol{\varepsilon}$ and the state variables at $t_n$, evaluate the *elastic trial state*

$$\boldsymbol{\varepsilon}^{e\,\mathrm{trial}}_{n+1} = \boldsymbol{\varepsilon}^e_n + \Delta\boldsymbol{\varepsilon}$$
$$\boldsymbol{\alpha}^{\mathrm{trial}}_{n+1} = \boldsymbol{\alpha}_n$$
$$\boldsymbol{\sigma}^{\mathrm{trial}}_{n+1} = \bar{\rho}\, \frac{\partial \psi}{\partial \boldsymbol{\varepsilon}^e}\bigg|^{\mathrm{trial}}_{n+1}, \quad \boldsymbol{A}^{\mathrm{trial}}_{n+1} = \bar{\rho}\, \frac{\partial \psi}{\partial \boldsymbol{\alpha}}\bigg|^{\mathrm{trial}}_{n+1}$$

(ii) Check for viscoplastic flow

IF $\Phi(\boldsymbol{\sigma}^{\mathrm{trial}}_{n+1}, \boldsymbol{A}^{\mathrm{trial}}_{n+1}) \leq 0$

THEN set $(\cdot)_{n+1} = (\cdot)^{\mathrm{trial}}_{n+1}$ and EXIT

(iii) Viscoplastic return mapping. Solve the system

$$\left\{\begin{array}{c} \boldsymbol{\varepsilon}^e_{n+1} - \boldsymbol{\varepsilon}^{e\,\mathrm{trial}}_{n+1} + \Delta\gamma\, \boldsymbol{N}(\boldsymbol{\sigma}_{n+1}, \boldsymbol{A}_{n+1}) \\ \boldsymbol{\alpha}_{n+1} - \boldsymbol{\alpha}^{\mathrm{trial}}_{n+1} - \Delta\gamma\, \boldsymbol{H}(\boldsymbol{\sigma}_{n+1}, \boldsymbol{A}_{n+1}) \end{array}\right\} = \left\{\begin{array}{c} \mathbf{0} \\ \mathbf{0} \end{array}\right\}$$

for $\boldsymbol{\varepsilon}^e_{n+1}$, and $\boldsymbol{\alpha}_{n+1}$ with

$$\Delta\gamma = \Delta\gamma(\boldsymbol{\sigma}_{n+1}, \boldsymbol{A}_{n+1}) = \Delta t\, \dot{\gamma}(\boldsymbol{\sigma}_{n+1}, \boldsymbol{A}_{n+1})$$

and

$$\boldsymbol{\sigma}_{n+1} = \bar{\rho}\, \frac{\partial \psi}{\partial \boldsymbol{\varepsilon}^e}\bigg|_{n+1}, \quad \boldsymbol{A}_{n+1} = \bar{\rho}\, \frac{\partial \psi}{\partial \boldsymbol{\alpha}}\bigg|_{n+1}$$

(iv) EXIT

the considered interval. Nevertheless, the terminology viscoplastic *return mapping* remains justifiable in the present case since, upon application of the procedure, the updated stress is obtained by moving (or *returning*) the trial stress towards the yield surface.

## 11.5.2. ALTERNATIVE EULER-BASED ALGORITHMS

Similarly to the rate-independent case (refer to Section 7.2.7, page 201), different numerical integration algorithms can be employed in the stress updating procedure. In what follows we list the basic equations of the generalised trapezoidal and midpoint algorithms. For further details on alternative integration algorithms we refer to Cormeau (1975), Zienkiewicz and Cormeau (1974), Hughes and Taylor (1978), Marques and Owen (1983), Peirce *et al.* (1984) and Kojić and Bathe (1987).

***The generalised trapezoidal algorithm***

Here, the backward Euler discrete equations of Box 11.4 are replaced with the following system

$$\begin{aligned} \varepsilon^e_{n+1} &= \varepsilon^e_n + \Delta\varepsilon - \Delta t\,[(1-\theta)\,\boldsymbol{G}_n + \theta\,\boldsymbol{G}_{n+1}] \\ \boldsymbol{\alpha}_{n+1} &= \boldsymbol{\alpha}_n + \Delta t\,[(1-\theta)\,\boldsymbol{J}_n + \theta\,\boldsymbol{J}_{n+1}], \end{aligned} \tag{11.72}$$

where $\theta$ is a prescribed parameter

$$0 \le \theta \le 1. \tag{11.73}$$

For the choice $\theta = 1$, the implicit algorithm of Box 11.4 is recovered and $\theta = 0$ corresponds to the explicit algorithm.

***The generalised midpoint algorithm***

For the generalised midpoint rule, the discrete system of equations reads

$$\begin{aligned} \varepsilon^e_{n+1} &= \varepsilon^e_n + \Delta\varepsilon - \Delta t\,\boldsymbol{G}_{n+\theta} \\ \boldsymbol{\alpha}_{n+1} &= \boldsymbol{\alpha}_n + \Delta t\,\boldsymbol{J}_{n+\theta}, \end{aligned} \tag{11.74}$$

where the prescribed parameter, $\theta$, also lies within the interval $[0, 1]$ and

$$\begin{aligned} \boldsymbol{G}_{n+\theta} &= \boldsymbol{G}((1-\theta)\boldsymbol{\sigma}_{n+1} + \theta\,\boldsymbol{\sigma}_n, (1-\theta)\boldsymbol{A}_n + \theta\,\boldsymbol{A}_{n+1}) \\ \boldsymbol{J}_{n+\theta} &= \boldsymbol{J}((1-\theta)\boldsymbol{\sigma}_{n+1} + \theta\,\boldsymbol{\sigma}_n, (1-\theta)\boldsymbol{A}_n + \theta\,\boldsymbol{A}_{n+1}). \end{aligned} \tag{11.75}$$

Again, for $\theta = 1$, the implicit algorithm of Box 11.4 is recovered and $\theta = 0$ defines the explicit algorithm.

### 11.5.3. GENERAL CONSISTENT TANGENT OPERATOR

To complete the requirements for the implementation of the model within an implicit finite element environment, the tangent modulus consistent with the general algorithm is needed. Let us then consider the algorithm of Box 11.4. Given all variables of the problem at $t_n$ and a prescribed time increment $\Delta t$, the task here is to find the exact tangent operator

$$\mathsf{D} \equiv \frac{\mathrm{d}\boldsymbol{\sigma}_{n+1}}{\mathrm{d}\boldsymbol{\varepsilon}_{n+1}} = \frac{\mathrm{d}\boldsymbol{\sigma}_{n+1}}{\mathrm{d}\Delta\boldsymbol{\varepsilon}}, \tag{11.76}$$

consistent with the stress updating procedure defined by the backward Euler algorithm of Box 11.4.

Analogously to the general procedure for the rate-independent case (refer to Section 7.4.4, from page 238), we start by linearising the system of time-discrete equations of Box 11.4. The linearised system reads

$$\begin{Bmatrix} \mathrm{d}\varepsilon^e + \Delta t\,\dfrac{\partial \boldsymbol{G}}{\partial \boldsymbol{\sigma}} : \mathrm{d}\boldsymbol{\sigma} + \Delta t\,\dfrac{\partial \boldsymbol{G}}{\partial \boldsymbol{A}} * \mathrm{d}\boldsymbol{A} \\ \mathrm{d}\boldsymbol{\alpha} - \Delta t\,\dfrac{\partial \boldsymbol{J}}{\partial \boldsymbol{\sigma}} * \mathrm{d}\boldsymbol{\sigma} - \Delta t\,\dfrac{\partial \boldsymbol{J}}{\partial \boldsymbol{A}} * \mathrm{d}\boldsymbol{A} \end{Bmatrix} = \begin{Bmatrix} \mathrm{d}\Delta\varepsilon \\ \mathbf{0} \end{Bmatrix}, \tag{11.77}$$



where the symbol * denotes the product of the appropriate type and the subscripts $n+1$ have been omitted for notational convenience. With the introduction of the differential relations (7.129) (page 239), the linearised system is equivalently written as

$$\begin{bmatrix} \mathsf{C} + \Delta t\,\dfrac{\partial \boldsymbol{G}}{\partial \boldsymbol{\sigma}} & \mathsf{B} + \Delta t\,\dfrac{\partial \boldsymbol{G}}{\partial \boldsymbol{A}} \\ \mathsf{A} - \Delta t\,\dfrac{\partial \boldsymbol{J}}{\partial \boldsymbol{\sigma}} & \mathsf{J} - \Delta t\,\dfrac{\partial \boldsymbol{J}}{\partial \boldsymbol{A}} \end{bmatrix} \begin{bmatrix} \mathrm{d}\boldsymbol{\sigma} \\ \mathrm{d}\boldsymbol{A} \end{bmatrix} = \begin{bmatrix} \mathrm{d}\Delta\boldsymbol{\varepsilon} \\ \mathbf{0} \end{bmatrix}. \tag{11.78}$$

By inverting the linearised system above, we finally obtain a tangent relation which can be written symbolically as

$$\begin{bmatrix} \mathrm{d}\boldsymbol{\sigma} \\ \mathrm{d}\boldsymbol{A} \end{bmatrix} = \begin{bmatrix} \mathsf{D}_{11} & \mathsf{D}_{12} \\ \mathsf{D}_{21} & \mathsf{D}_{22} \end{bmatrix} \begin{bmatrix} \mathrm{d}\Delta\boldsymbol{\varepsilon} \\ \mathbf{0} \end{bmatrix}, \tag{11.79}$$

where $\mathsf{D}_{ij}$ are tensors of appropriate order resulting from the inversion of (11.78). The consistent tangent operator we are looking for is the fourth-order tensor

$$\mathsf{D} \equiv \frac{\mathrm{d}\boldsymbol{\sigma}_{n+1}}{\mathrm{d}\Delta\boldsymbol{\varepsilon}} = \mathsf{D}_{11}. \tag{11.80}$$

***Models with a yield surface***

For models with a yield surface, the tangent modulus is elastic if the state is within the elastic domain; that is, as in rate-independent plasticity, when $\Phi(\boldsymbol{\sigma}_{n+1}, \boldsymbol{A}_{n+1}) \le 0$, we have

$$\mathsf{D} = \mathsf{D}^e = \bar{\rho}\frac{\partial^2 \psi}{\partial \varepsilon^{e2}}. \tag{11.81}$$

Under viscoplastic flow, i.e. when $\Phi(\boldsymbol{\sigma}_{n+1}, \boldsymbol{A}_{n+1}) > 0$, the stress is the result from the solution of the equation system of item (iii) of Box 11.5. In this case, the tangent operator is a specialisation of the general tangent modulus (11.80) where the functions $\boldsymbol{G}$ and $\boldsymbol{J}$ taking part in the symbolic matrix (11.78) are defined by (11.71). The derivatives of $\boldsymbol{G}$ then specialise as

$$\begin{aligned} \frac{\partial \boldsymbol{G}}{\partial \boldsymbol{\sigma}} &= \dot{\gamma}\,\frac{\partial \boldsymbol{N}}{\partial \boldsymbol{\sigma}} + \boldsymbol{N} \otimes \frac{\partial \dot{\gamma}}{\partial \boldsymbol{\sigma}} \\ \frac{\partial \boldsymbol{G}}{\partial \boldsymbol{A}} &= \dot{\gamma}\,\frac{\partial \boldsymbol{N}}{\partial \boldsymbol{A}} + \boldsymbol{N} * \frac{\partial \dot{\gamma}}{\partial \boldsymbol{A}}. \end{aligned} \tag{11.82}$$

Similarly, the derivatives of $\boldsymbol{J}$ specialise as

$$\begin{aligned} \frac{\partial \boldsymbol{J}}{\partial \boldsymbol{\sigma}} &= \dot{\gamma}\,\frac{\partial \boldsymbol{H}}{\partial \boldsymbol{\sigma}} + \boldsymbol{H} * \frac{\partial \dot{\gamma}}{\partial \boldsymbol{\sigma}} \\ \frac{\partial \boldsymbol{J}}{\partial \boldsymbol{A}} &= \dot{\gamma}\,\frac{\partial \boldsymbol{H}}{\partial \boldsymbol{A}} + \boldsymbol{H} * \frac{\partial \dot{\gamma}}{\partial \boldsymbol{A}}. \end{aligned} \tag{11.83}$$

## 11.6. Application: computational implementation of a von Mises-based model

To illustrate the application of the above numerical framework, this section describes in detail the basic ingredients of the computational implementation of the von Mises-based model with isotropic strain hardening given in Box 11.2. In addition to the detailed description of the associated integration algorithm and consistent tangent operator, we present an accuracy analysis of the algorithm based on iso-error maps. We remark that the procedures presented here are *not* incorporated in the standard version of program HYPLAS that accompanies this book.

### 11.6.1. INTEGRATION ALGORITHM

The integration algorithm described here is a specialisation of the generic algorithm described in Section 11.5 to the model whose constitutive equations are summarised in Box 11.2. The algorithm comprises the standard *elastic predictor* and the *viscoplastic return mapping* which, for the present model, has the following format.

1. *Elastic predictor*. The material is assumed to behave purely elastically within the time interval $[t_n, t_{n+1}]$. The *elastic trial* state is then computed as

$$\begin{aligned} \boldsymbol{\varepsilon}^{e\,\mathrm{trial}} &= \boldsymbol{\varepsilon}^e_n + \Delta\boldsymbol{\varepsilon} \\ \boldsymbol{\varepsilon}^{p\,\mathrm{trial}} &= \boldsymbol{\varepsilon}^p_n \\ \bar{\varepsilon}^{p\,\mathrm{trial}} &= \bar{\varepsilon}^p_n \\ \boldsymbol{\sigma}^{\mathrm{trial}} &= \mathbf{D}^e : \boldsymbol{\varepsilon}^{e\,\mathrm{trial}}. \end{aligned} \tag{11.84}$$

If $\Phi(\boldsymbol{\sigma}^{\mathrm{trial}}, \sigma_y(\bar{\varepsilon}^{p\,\mathrm{trial}})) \leq 0$, then the process is indeed elastic within the interval and the variables at $t_{n+1}$ are assigned the values of the trial variables. Otherwise, we apply the viscoplastic return-mapping algorithm described in the following.

2. *Viscoplastic return mapping*. At this stage, we solve the system of discretised equations of item (iii) of Box 11.5 which, for the present model, by taking the linear elastic law into consideration, are specialised as

$$\begin{aligned} \boldsymbol{\sigma}_{n+1} &= \boldsymbol{\sigma}^{\mathrm{trial}} - \Delta\gamma\, \mathbf{D}^e : \left.\frac{\partial \Phi}{\partial \boldsymbol{\sigma}}\right|_{n+1} \\ \bar{\varepsilon}^p_{n+1} &= \bar{\varepsilon}^p_n + \Delta\gamma, \end{aligned} \tag{11.85}$$

where the *incremental multiplier*, $\Delta\gamma$, is given by

$$\Delta\gamma = \frac{\Delta t}{\mu}\left[\left(\frac{q(\boldsymbol{\sigma}_{n+1})}{\sigma_y(\bar{\varepsilon}^p_{n+1})}\right)^{1/\epsilon} - 1\right], \tag{11.86}$$

with $\Delta t$ denoting the time increment within the considered interval. After solving (11.85), we can update

$$\boldsymbol{\varepsilon}^p_{n+1} = \boldsymbol{\varepsilon}^p_n + \Delta\gamma \left.\frac{\partial \Phi}{\partial \boldsymbol{\sigma}}\right|_{n+1}, \quad \boldsymbol{\varepsilon}^e_{n+1} = \boldsymbol{\varepsilon}^{e\,\mathrm{trial}} - \Delta\gamma \left.\frac{\partial \Phi}{\partial \boldsymbol{\sigma}}\right|_{n+1}. \tag{11.87}$$



***Single-equation corrector***

The viscoplastic corrector can be more efficiently implemented by reducing (11.85) to a single scalar equation. The situation here is completely analogous to that of the implementation of the elastoplastic (rate-independent) von Mises model described in Section 7.3.2 (page 217). For convenience, the steps leading to the system reduction are repeated here. Firstly, we observe that the plastic flow vector

$$\frac{\partial \Phi}{\partial \boldsymbol{\sigma}} = \sqrt{\frac{3}{2}}\,\frac{\boldsymbol{s}}{\|\boldsymbol{s}\|} \tag{11.88}$$

is deviatoric so that the hydrostatic stress is independent of the viscoplastic flow. The stress update equation $(11.85)_1$ can then be split as

$$\begin{aligned} \boldsymbol{s}_{n+1} &= \boldsymbol{s}^{\mathrm{trial}} - \Delta\gamma\, 2G \sqrt{\frac{3}{2}}\,\frac{\boldsymbol{s}_{n+1}}{\|\boldsymbol{s}_{n+1}\|} \\ p_{n+1} &= p^{\mathrm{trial}}. \end{aligned} \tag{11.89}$$

Further, simple inspection of $(11.89)_1$ shows that $\boldsymbol{s}_{n+1}$ is a scalar multiple of $\boldsymbol{s}^{\mathrm{trial}}$ so that, trivially, we have the identity

$$\frac{\boldsymbol{s}_{n+1}}{\|\boldsymbol{s}_{n+1}\|} = \frac{\boldsymbol{s}^{\mathrm{trial}}}{\|\boldsymbol{s}^{\mathrm{trial}}\|}, \tag{11.90}$$

which allows us to rewrite $(11.89)_1$ as

$$\boldsymbol{s}_{n+1} = \left(1 - \sqrt{\frac{3}{2}}\,\frac{\Delta\gamma\, 2G}{\|\boldsymbol{s}^{\mathrm{trial}}\|}\right)\boldsymbol{s}^{\mathrm{trial}} = \left(1 - \frac{\Delta\gamma\, 3G}{q^{\mathrm{trial}}}\right)\boldsymbol{s}^{\mathrm{trial}} \tag{11.91}$$

where $q^{\mathrm{trial}}$ is the elastic trial von Mises equivalent stress. Application of the definition of the von Mises equivalent stress to the above equation gives the update formula

$$q_{n+1} = q^{\mathrm{trial}} - 3G\,\Delta\gamma. \tag{11.92}$$

Finally, with the substitution of the above formula together with $(11.85)_2$ into (11.86) we obtain the following scalar algebraic equation for the multiplier $\Delta\gamma$

$$\Delta\gamma - \frac{\Delta t}{\mu}\left[\left(\frac{q^{\mathrm{trial}} - 3G\,\Delta\gamma}{\sigma_y(\bar{\varepsilon}^p_n + \Delta\gamma)}\right)^{1/\epsilon} - 1\right] = 0, \tag{11.93}$$

or, equivalently, after a straightforward rearrangement,

$$(q^{\mathrm{trial}} - 3G\,\Delta\gamma)\left(\frac{\Delta t}{\mu\,\Delta\gamma + \Delta t}\right)^{\epsilon} - \sigma_y(\bar{\varepsilon}^p_n + \Delta\gamma) = 0. \tag{11.94}$$

The single-equation viscoplastic corrector comprises the solution of (11.93) or (11.94) for the unknown $\Delta\gamma$ followed by the straightforward update of $\boldsymbol{\sigma}$, $\bar{\varepsilon}^p$, $\boldsymbol{\varepsilon}^p$, $\boldsymbol{\varepsilon}^e$ according to the relevant formulae. The solution of the equation for $\Delta\gamma$ is, as usual, undertaken by the Newton–Raphson iterative scheme. The overall algorithm is summarised in Box 11.6 in pseudo-code format.

**Box 11.6.** Integration algorithm for von Mises-type viscoplastic model (over a generic time interval $[t_n, t_{n+1}]$ with $\Delta t = t_{n+1} - t_n$).

(i) Elastic predictor. Given $\Delta\boldsymbol{\varepsilon}$, and the state variables at $t_n$, evaluate the *elastic trial state*

$$\boldsymbol{\varepsilon}^{e\,\mathrm{trial}} := \boldsymbol{\varepsilon}^e_n + \Delta\boldsymbol{\varepsilon}$$
$$\bar{\varepsilon}^{p\,\mathrm{trial}}_{n+1} := \bar{\varepsilon}^p_n$$
$$p^{\mathrm{trial}}_{n+1} := K\,\varepsilon^{e\,\mathrm{trial}}_{\mathrm{v}\,n+1}; \quad \boldsymbol{s}^{\mathrm{trial}} := 2G\,\boldsymbol{\varepsilon}^{e\,\mathrm{trial}}_{\mathrm{d}\,n+1}$$
$$q^{\mathrm{trial}}_{n+1} := \sqrt{\tfrac{3}{2}}\,\|\boldsymbol{s}^{\mathrm{trial}}_{n+1}\|$$

(ii) Check for viscoplastic flow

IF $\quad q^{\mathrm{trial}}_{n+1} - \sigma_y(\bar{\varepsilon}^{p\,\mathrm{trial}}_{n+1}) \le 0 \quad$ (elastic step)

THEN set $\quad (\cdot)_{n+1} := (\cdot)^{\mathrm{trial}}_{n+1} \quad$ and EXIT

(iii) Viscoplastic flow. Solve the return-mapping equation

$$R(\Delta\gamma) \equiv (q^{\mathrm{trial}}_{n+1} - 3G\,\Delta\gamma)\left(\frac{\Delta t}{\mu\,\Delta\gamma + \Delta t}\right)^{\epsilon} - \sigma_y(\bar{\varepsilon}^p_n + \Delta\gamma) = 0$$

for $\Delta\gamma$ using the Newton–Raphson scheme. Then update

$$p_{n+1} := p^{\mathrm{trial}}_{n+1}; \quad \boldsymbol{s}_{n+1} := \left(1 - \frac{\Delta\gamma\,3G}{q^{\mathrm{trial}}_{n+1}}\right)\boldsymbol{s}^{\mathrm{trial}}_{n+1}$$
$$\boldsymbol{\sigma}_{n+1} := \boldsymbol{s}_{n+1} + p_{n+1}\,\boldsymbol{I}$$
$$\boldsymbol{\varepsilon}^e_{n+1} := \frac{1}{2G}\,\boldsymbol{s}_{n+1} + \frac{1}{3}\,\varepsilon^{e\,\mathrm{trial}}_{\mathrm{v}\,n+1}\,\boldsymbol{I}$$
$$\bar{\varepsilon}^p_{n+1} := \bar{\varepsilon}^p_n + \Delta\gamma$$

(iv) EXIT

**Remark 11.4 (Rate-independent limit).** Note that, as expected, equation (11.94) rigorously recovers its elastoplastic (rate-independent) counterpart (7.91) (refer to page 219) when $\mu \to 0$ (no viscosity), $\epsilon \to 0$ (no rate-sensitivity) or $\Delta t \to \infty$ (infinitely slow straining). Clearly, in such cases, the algorithm of Box 11.6 reproduces the rate-independent elastoplastic numerical solution.

**Remark 11.5 (Computational implementation aspects).** In the computer implementation of the model (as shown in Box 11.6), it is more convenient to solve (11.94) rather than (11.93) in the viscoplastic corrector stage of the algorithm. The reason for this lies in the fact that, for low rate-sensitivity, i.e. small values of $\epsilon$, the Newton–Raphson scheme for solution of (11.93) becomes unstable as its convergence bowl is sharply reduced with decreasing $\epsilon$. The reduction of the convergence bowl stems from the fact that large exponents $1/\epsilon$ can easily produce numbers which are computationally intractable. This fact has been recognised by Perić (1993) in the context of a more general viscoplastic algorithm. In equation (11.94), on the other hand,



the term to the power $\epsilon$ on the left-hand side can only assume values within the interval $[0, 1]$ and causes no numerical problems within practical ranges of material constants.

**Remark 11.6 (Solution existence and uniqueness).** Within a viscoplastic step, we have

$$q^{\mathrm{trial}} > \sigma_y(\bar{\varepsilon}^{p\,\mathrm{trial}}) = \sigma_y(\bar{\varepsilon}^p_n).$$

Let $R(\Delta\gamma)$ be the function defined by the right-hand side of (11.94). The above inequality clearly implies that $R(0) > 0$. In addition, taking into account the strict positiveness of the hardening function $\sigma_y$, we can easily verify that $R(q^{\mathrm{trial}}/3G) < 0$. The continuity of $R$ then implies that (11.94) has a root within the interval $(0, q^{\mathrm{trial}}/3G)$. Let us now consider the derivative of $R$,

$$R'(\Delta\gamma) = -\left(3G + \epsilon\mu\,\frac{q^{\mathrm{trial}} - 3G\Delta\gamma}{\mu\,\Delta\gamma + \Delta t}\right)\left(\frac{\Delta t}{\mu\,\Delta\gamma + \Delta t}\right)^{\epsilon} - H(\bar{\varepsilon}^p_n + \Delta\gamma),$$

where $H$ is the derivative of the isotropic hardening function $\sigma_y$. Upon simple inspection, we can easily establish that the derivative $R'$ is strictly negative for $\Delta\gamma \in (0, q^{\mathrm{trial}}/3G)$ if the viscoplastic model is *non-softening*, i.e. if $H$ is non-negative for any value of accumulated plastic strain. The strict negativeness of $R'$ in conjunction with the existence of a root for $R$ established in the above implies that the root of $R$ (the solution of the viscoplastic corrector equation) within the interval $(0, q^{\mathrm{trial}}/3G)$ is unique for non-softening materials.

### 11.6.2. ISO-ERROR MAPS

To illustrate the accuracy of the above integration algorithm in practical situations, this section presents some iso-error maps, produced with material constants covering a range of high rate-sensitivity to rate-independence. The material is assumed perfectly viscoplastic (no hardening). The maps have been generated in the standard fashion as described in Section 7.2.10 (refer to Figure 7.7, page 215). Using the three-dimensional implementation of the model, we start from a stress point at time $t_n$, with $\boldsymbol{\sigma}_n$ lying on the yield surface, and apply a sequence of strain increments (at *constant strain rate* within the interval $[t_n, t_{n+1}]$), corresponding to linear combinations of trial stress increments in the direction normal and tangential (directions of the unit tensors $\boldsymbol{N}$ and $\boldsymbol{T}$ of Figure 7.7, respectively) to the von Mises circle in the deviatoric plane. Figures 11.5 and 11.6 show iso-error maps obtained at low and high strain rates with the non-dimensional rate

$$\mu\,\|\dot{\boldsymbol{\varepsilon}}\|$$

set respectively to 1 and 1000. For each non-dimensional rate, three values of rate-sensitivity parameter, $\epsilon$, have been used: $10^0$, $10^{-1}$ and 0. Recall that for $\epsilon = 0$ the algorithm reproduces the rate-independent solution. The resulting map in this case is obviously identical to the rate-independent map of Figure 7.7(b) and is shown here only to emphasise the effect of rate-dependence on the integration error. The main conclusion drawn from the iso-error maps is that, in general, increasing (decreasing) rate-sensitivity and/or increasing (decreasing) strain rates tend to produce decreasing (increasing) integration errors. The largest errors are expected in the rate-independent limit.

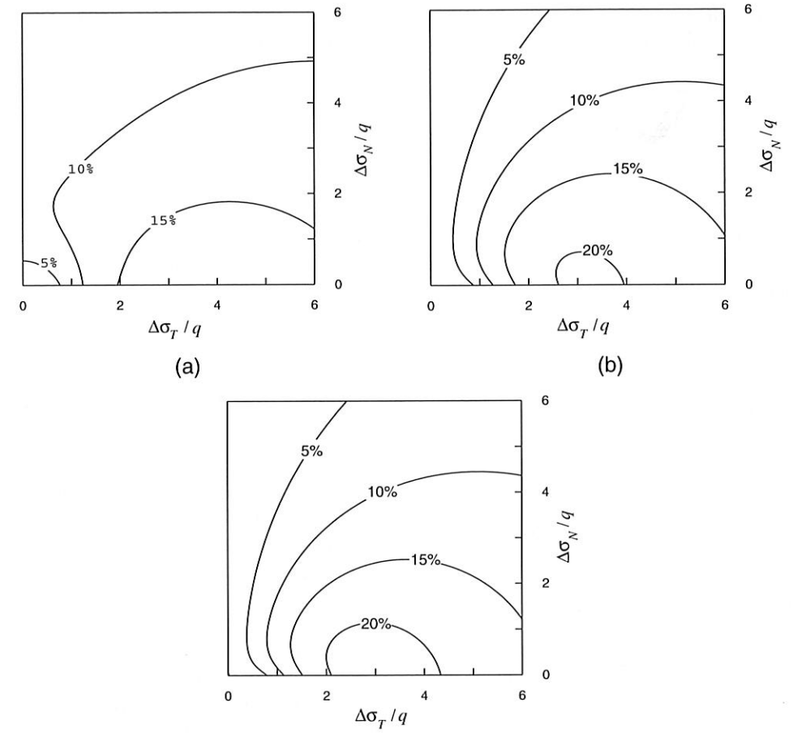


**Figure 11.5.** Iso-error maps with $\mu \, \|\dot{\varepsilon}\| = 1$; (a) $\epsilon = 10^0$; (b) $\epsilon = 10^{-1}$; (c) $\epsilon = 0$ (rate-independent).

### 11.6.3. CONSISTENT TANGENT OPERATOR

The consistent tangent operator here is a particular case of the general tangent operator derived in Section 11.5.3. Clearly, when the stress state lies within the elastic domain and no viscoplastic flow is possible, the tangent operator is the elastic tangent, $\mathsf{D}^e$. Under viscoplastic flow, the tangent operator which (as in the rate-independent case) will be denoted $\mathsf{D}^{ep}$, is derived by consistently linearising the viscoplastic return-mapping algorithm referred to in item (iii) of Box 11.6. Its closed-form expression can be obtained by following the same steps of the derivation of the elastoplastic (rate-independent) tangent presented in Section 7.4.2 (from page 232). The incremental constitutive function for the stress tensor in the present case has identical format to that of the rate-independent implementation given by (7.93) – which reduces to (7.113) under plastic flow – but the incremental plastic multiplier $\Delta\gamma$ here is the solution of viscoplastic return-mapping equation (11.94). Thus, to obtain the viscoplastic consistent tangent, we simply replace the derivative of the incremental plastic



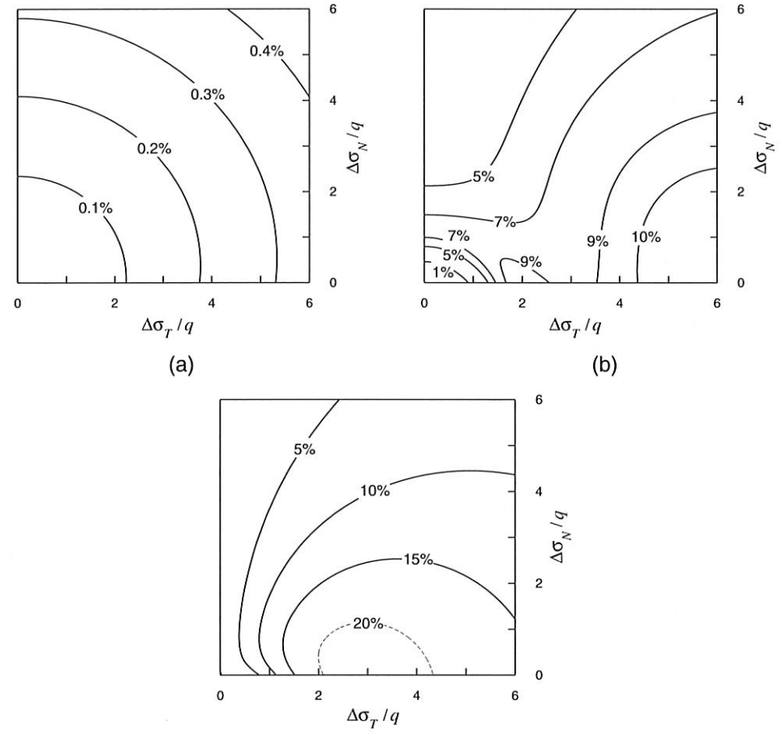


**Figure 11.6.** Iso-error maps with $\mu \, \|\dot{\varepsilon}\| = 10^3$; (a) $\epsilon = 10^0$; (b) $\epsilon = 10^{-1}$; (c) $\epsilon = 0$ (rate-independent).

multiplier (7.118) with the expression

$$\frac{\partial \Delta\gamma}{\partial \varepsilon^{e\,\mathrm{trial}}_{n+1}} = \frac{2G\sqrt{\frac{3}{2}}}{3G + \left(\frac{\Delta t}{\mu\,\Delta\gamma + \Delta t}\right)^{-\epsilon} H + \frac{\epsilon\mu\, q_{n+1}}{\mu\,\Delta\gamma + \Delta t}} \bar{\boldsymbol{N}}_{n+1}, \tag{11.95}$$

which is consistent with (11.94). Analogously to the elastoplastic case, this expression is obtained by taking the differential of the viscoplastic corrector equation (11.94), having $\Delta\gamma$ and $q^{\mathrm{trial}}_{n+1}$ as variables, and equating it to zero. With the above differential relation, the final

elasto-viscoplastic consistent tangent operator is obtained in closed form as

$$\mathsf{D}^{ep} = 2G\left(1 - \frac{\Delta\gamma\, 3G}{q^{\text{trial}}_{n+1}}\right)\mathsf{I}_{\text{d}} + 6G^2\left[\frac{\Delta\gamma}{q^{\text{trial}}_{n+1}} - \frac{1}{3G + \left(\frac{\Delta t}{\mu\,\Delta\gamma+\Delta t}\right)^{-\epsilon} H + \frac{\epsilon\mu\, q_{n+1}}{\mu\,\Delta\gamma+\Delta t}}\right]\bar{\boldsymbol{N}}_{n+1}\otimes\bar{\boldsymbol{N}}_{n+1} + K\,\boldsymbol{I}\otimes\boldsymbol{I}. \tag{11.96}$$

Note that the tangent operator is symmetric.

**Remark 11.7 (Rate-independent limit).** By simple inspection we find that in the limits $\epsilon \to 0$ (vanishing rate-sensitivity parameter), $\mu \to 0$ (vanishing viscosity) or $\Delta t \to \infty$ (infinitely slow straining), expression (11.96) rigorously recovers the elastoplastic consistent tangent operator of the isotropically hardening rate-independent von Mises model with implicit return mapping given by expression (7.120).

### 11.6.4. PERZYNA-TYPE MODEL IMPLEMENTATION

The implementation of the von Mises-based model with Perzyna's viscoplastic law (11.40) follows exactly the same procedure as described in the above except that, consistently with the backward Euler time discretization of (11.40), the return-mapping equation (11.94) (or item (iii) of Box 11.6) is replaced with

$$q^{\text{trial}} - 3G\,\Delta\gamma - \left[1 + \left(\frac{\mu\,\Delta\gamma}{\Delta t}\right)^{\epsilon}\right]\sigma_y(\bar{\varepsilon}^p_n + \Delta\gamma) = 0. \tag{11.97}$$

Here, we have assumed isotropic strain hardening. Note that, as $\mu \to \infty$ (vanishing viscosity) or $\Delta t \to \infty$ (infinitely slow process) equation (11.97) reduces to that of the elastoplastic rate-independent von Mises model with yield stress $\sigma_y$. For vanishing rate sensitivity parameter, $\epsilon \to 0$, (11.97) reduces to a von Mises elastoplastic return-mapping equation with yield stress $2\sigma_y$. This is, as one should expect, in agreement with the theoretical limits of the Perzyna model discussed in the text immediately following equation (11.40).

#### *Elasto-viscoplastic consistent tangent operator*

The differential relation between the incremental plastic multiplier and $\boldsymbol{\varepsilon}^{e\,\text{trial}}_{n+1}$ consistent with the return-mapping equation (11.97) reads

$$\frac{\partial\Delta\gamma}{\partial\boldsymbol{\varepsilon}^{e\,\text{trial}}_{n+1}} = \frac{2G\sqrt{\frac{3}{2}}}{3G + \left[1 + \left(\frac{\mu\,\Delta\gamma}{\Delta t}\right)^{\epsilon}\right]H + \frac{\epsilon\mu}{\Delta t}\left(\frac{\mu\,\Delta\gamma}{\Delta t}\right)^{\epsilon-1}\sigma_y}\,\bar{\boldsymbol{N}}_{n+1}, \tag{11.98}$$



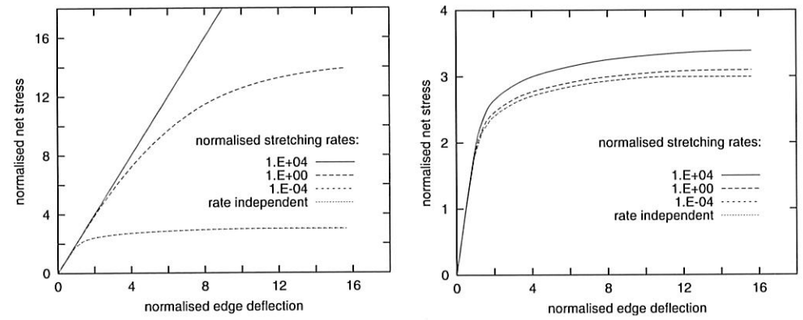


**Figure 11.7.** Double-notched specimen. Reaction–deflection diagrams: (a) $\epsilon = 10^0$; (b) $\epsilon = 10^{-2}$.

where $\sigma_y$ is evaluated at $\bar{\varepsilon}^p_{n+1} = \bar{\varepsilon}^p_n + \Delta\gamma$. This expression is the counterpart of (11.95) for the present implementation of Perzyna's viscoplasticity law. The corresponding elasto-viscoplastic consistent tangent operator is obtained following the usual procedure as

$$\mathsf{D}^{ep} = 2G\left(1 - \frac{\Delta\gamma\, 3G}{q^{\text{trial}}_{n+1}}\right)\mathsf{I}_{\text{d}} + 6G^2\left[\frac{\Delta\gamma}{q^{\text{trial}}_{n+1}} - \frac{1}{3G + \left[1 + \left(\frac{\mu\,\Delta\gamma}{\Delta t}\right)^{\epsilon}\right]H + \frac{\epsilon\mu}{\Delta t}\left(\frac{\mu\,\Delta\gamma}{\Delta t}\right)^{\epsilon-1}\sigma_y}\right]\bar{\boldsymbol{N}}_{n+1}\otimes\bar{\boldsymbol{N}}_{n+1} + K\,\boldsymbol{I}\otimes\boldsymbol{I}. \tag{11.99}$$

Its format is completely analogous to that of (11.96).

## 11.7. Examples

The finite element examples presented in this section illustrate applications of the computational treatment of viscoplasticity described above. The underlying viscoplastic material model is the one shown in Box 11.2, which includes isotropic strain hardening.

### 11.7.1. DOUBLE-NOTCHED TENSILE SPECIMEN

The rate-independent version of this problem has been studied in Section 7.5.5 (from page 255). The problem consists of the plane strain analysis of a deep double-notched tensile specimen. The geometry of the specimen and the finite element mesh used are shown in Figure 7.29 (page 256). Analogously to the prescription of edge displacement $u$ (refer to Figure 7.29), the simulation consists of stretching the specimen by prescribing a constant (in time) vertical velocity $v$ on the top nodes of the mesh. For convenience, we define the normalised stretching rate

$$v^* = \frac{\mu\, v}{l/2}$$

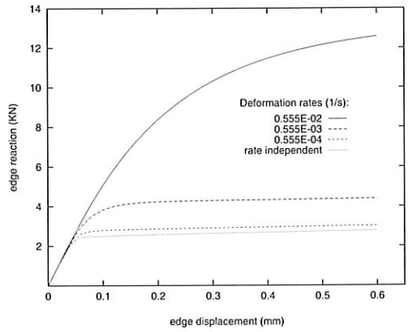


(a)

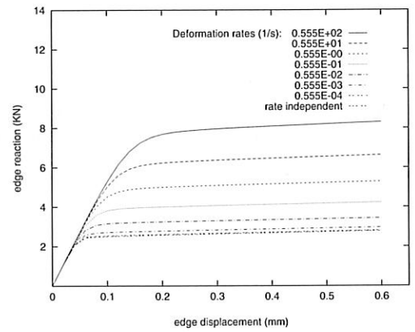


(b)

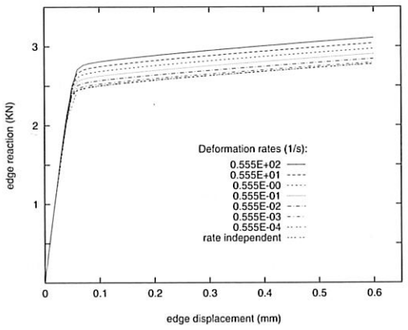


(c)

**Figure 11.8.** Stretching of a perforated plate. Displacement-reaction diagrams. (a) $\epsilon = 10^0$; (b) $\epsilon = 10^{-1}$; (c) $\epsilon = 10^{-2}$.



and the simulation is carried out for three different values of $v^*$

$$v^* = 10^{-4},\ 10^0,\ 10^4.$$

This choice covers very slow to very fast strain rates and is meant to demonstrate the robustness of the integration algorithm over a wide range of strain rates. The following material parameters are adopted

$$E = 206.9\,\text{GPa}; \quad \nu = 0.29; \quad \sigma_y = 0.45\,\text{GPa (constant)}.$$

The linearly hardening case listed in Figure 7.29 is not considered here. In order to show the effect of the rate-sensitivity parameter on the behaviour of the model, two values of $\epsilon$ are considered

$$\epsilon = 10^0 \quad \text{and} \quad 10^{-2}.$$

The results of the finite element simulations are presented in Figure 11.7 whose diagrams show the evolution of the reaction forces on the constrained edge against the corresponding edge deflection. As in the rate-independent case, the results are plotted in terms of the *normalised net stress* and the *normalised edge deflection* defined in Section 7.5.5. The results for $\epsilon = 10^0$ and $10^{-2}$ are shown, respectively, in Figures 11.7(a) and (b). They illustrate the expected higher reactions and limit loads for higher rates of stretching. For the lowest non-dimensional rate of $10^{-4}$, the rate-independent solution is recovered for any rate-sensitivity parameter. We remark that the rate-independent solution shown in the graphs for comparison can be obtained with the present model/algorithm simply by setting $\epsilon = 0$ or $\mu = 0$.

### 11.7.2. PLANE STRESS: STRETCHING OF A PERFORATED PLATE

This section describes the viscoplastic version of the plane stress problem of Section 9.5.3 (from page 390). This example has been analysed by Perić (1993). Here, a plane stress version of the numerical integration algorithm discussed in Section 11.6.1 is employed. The plane stress implementation adopted follows the nested iteration approach described in Section 9.2.2 (page 362) in the context of rate-independent plasticity. The problem consists of the axial stretching at constant rate of a perforated rectangular plate whose geometry is shown in Figure 9.7 (page 392). The mesh, boundary conditions and the material parameters that are common to both plastic and viscoplastic models are also shown in Figure 9.7. Note that linear strain hardening is assumed. The viscosity parameter adopted (required for the viscoplastic model) is

$$\mu = 500\,\text{s}.$$

Similarly to the previous example, in order to illustrate the response predicted by the viscoplastic model over a wide range of conditions, several simulations are carried out with various stretching rates, with three values of rate sensitivity coefficients ($\epsilon = 1, 10^{-1}, 10^{-2}$) being considered. The results obtained in the simulations are shown in Figure 11.8 where the reaction on the constrained edge of the plate is plotted against the prescribed edge displacement for the various conditions considered. The stretching rate in the present case is defined as

$$2v/l,$$

where $v$ is the stretching velocity imposed on the nodes of the upper edge. The three graphs of Figure 11.8 show the effect of stretching rates on the response of the plate, with higher reactions obtained at high rates and the rate-independent solution being approached as the stretching rate vanishes. The effects of the rate sensitivity parameter are also clearly illustrated. At higher (lower) values of $\epsilon$, a greater (smaller) variation of reaction as a function of the stretching rate is produced.

# 12 DAMAGE MECHANICS

INTERNAL damage can be defined as the presence and evolution of cracks and cavities at the microscopic level which may, eventually, lead to failure – a complete loss of load-carrying capability of the material. In many engineering applications, particularly those where mechanical/structural components are subjected to severe service conditions, the useful life of components is a crucial item of information which has to be carefully considered during the design process. In such cases, the ability of the designer to predict mechanical failure becomes an important factor. In some applications, such as in certain types of industrial machinery, non-scheduled stops for maintenance owing to unpredicted failure may incur serious economic consequences. In the design of manufacturing processes, such as metal-forming operations, prediction of failure is also a crucial issue. In safety-critical applications, frequently encountered in the aeronautical and nuclear industries, unpredicted failure may have catastrophic effects with consequences far beyond purely economical issues.

Traditionally, the prediction of useful life/failure of materials is based on mostly empirical experience accumulated over long periods of time. In some cases, failure prediction is achieved by the systematic (and expensive) testing of real models under laboratory-reproduced service conditions. However, with the growing knowledge of the mechanisms of progressive internal damage that cause failure in a wide range of materials, it is becoming possible to formulate continuum constitutive models capable of accounting for the evolution of internal deterioration. This relatively new branch of continuum solid mechanics is known as *Continuum Damage Mechanics* (*CDM*). This fact, allied to the fast development of computational mechanics techniques, has made the use of computational tools to carry out life/failure prediction a realistic alternative that can be successfully adopted in many design and damage assessment situations.

The present chapter is devoted to computational continuum damage mechanics. Our intention here is to provide the reader with an introduction to this new and promising ramification of computational solid mechanics that has been gaining widespread acceptance over the last two decades. The material presented in this chapter is summarised as follows. After providing a brief review of some basic mechanisms that characterise the presence and evolution of damage in Section 12.1, we give in Section 12.2 a brief historical account of CDM together with a discussion on the continuum modelling of damage phenomena. Sections 12.3, 12.4 and 12.5, describe, respectively, Lemaitre's ductile damage model (Lemaitre, 1985b), a simplified version of Lemaitre's model where kinematic hardening is not considered and Gurson's void growth model (Gurson, 1977). In each of these sections, the computational implementation of the corresponding constitutive models within an implicit finite element environment is described in detail. Note that the simplified version of Lemaitre's model discussed in Section 12.4 is fully incorporated into program `HYPLAS`. Further issues, including crack closure effects and damage anisotropy are addressed in Section 12.6.

*Computational Methods for Plasticity: Theory and Applications* EA de Souza Neto, D Perić and DRJ Owen